Geomechanics and Engineering, *Vol. 34, No. 5 (2023) 507-527*
https://doi.org/10.12989/gae.2023.34.5.507

Predicting the Young's modulus of frozen sand using machine learning approaches: State-of-the-art review

Reza Sarkhani Benemaran[1] and Mahzad Esmaeili-Falak*[2]

[1]*Department of Civil Engineering, Faculty of Geotechnical Engineering, University of Zanjan, Zanjan, Iran*
[2]*Department of Civil Engineering, North Tehran Branch, Islamic Azad University, Tehran, Iran*

(*Received December 16, 2022, Revised July 22, 2023, Accepted July 28, 2023*)

Abstract. Accurately estimation of the geo-mechanical parameters in Artificial Ground Freezing (AGF) is a most important scientific topic in soil improvement and geotechnical engineering. In order for this, one way is using classical and conventional constitutive models based on different theories like critical state theory, Hooke's law, and so on, which are time-consuming, costly, and troublous. The others are the application of artificial intelligence (AI) techniques to predict considered parameters and behaviors accurately. This study presents a comprehensive data-mining-based model for predicting the Young's Modulus of frozen sand under the triaxial test. For this aim, several single and hybrid models were considered including additive regression, bagging, M5-Rules, M5P, random forests (RF), support vector regression (SVR), locally weighted linear (LWL), gaussian process regression (GPR), and multi-layered perceptron neural network (MLP). In the present study, cell pressure, strain rate, temperature, time, and strain were considered as the input variables, where the Young's Modulus was recognized as target. The results showed that all selected single and hybrid predicting models have acceptable agreement with measured experimental results. Especially, hybrid Additive Regression-Gaussian Process Regression and Bagging-Gaussian Process Regression have the best accuracy based on Model performance assessment criteria.

Keywords: Artificial Ground Freezing; data mining; forecasting; laboratory test; numerical simulation

1. Introduction

Soil has always been considered as the oldest building material and the use of the Artificial Ground Freezing (AGF) technique has been considered more as a newer building material today. During recent decades, the AGF has widely been developed in geotechnical engineering because of the high demand for using underground spaces in municipal areas to provide risk-free and controlled premier in underground construction projects (Wood 2003, Esmaeili-Falak and Hajialilue-Bonab 2012, Choobar *et al.* 2013, Moradi *et al.* 2022, Esmaeili-Falak and Sarkhani Benemaran 2022). AGF is preferred over other soil improvement techniques due to technical and environmental (and sometimes economic) benefits, however, it may be the sole usable technique in special conditions (Andersland and Ladanyi 2003, Esmaeili-Falak *et al.* 2018). Therefore, perception of the essential parameters and constitutive modeling of the frozen soil is of particular importance which the use of artificial intelligence and regression analysis has been recently more considered for predicting the mechanical properties of frozen soils.

Numerous laboratory studies have been performed to investigate the behavior of frozen soils (Goughnour and Andersland 1968, Chai *et al.* 2017, Török *et al.* 2019, Mohan *et al.* 2019, Akhtar and Li 2020, Hou *et al.* 2020, Sarkhani Benemaran *et al.* 2022a). Nowadays, extensive Artificial Intelligence based models have been employed in various fields of civil engineering (Johari *et al.* 2006, Johari *et al.* 2011, Johari and Golkarfard 2018, Habibagahi *et al.* 2020, Johari and Fooladi 2020, Dehghanbanadaki *et al.* 2022, Sarkhani Benemaran *et al.* 2022b, Johari *et al.* 2021a, Johari *et al.* 2021b, Alzabeebee *et al.* 2022, Dinarvand and Ardakani 2022, Johari and Fooladi 2022, Ge *et al.* 2022, Lawal *et al.* 2022, Kim *et al.* 2022, Kwak and Ko 2022, Mahmoodzadeh *et al.* 2022a, Sun and Liu 2022, Yan 2022, Zhang *et al.* 2022, Mahmoodzadeh *et al.* 2022b, Esmaeili-Falak and Sarkhani Benemarn 2023, Dawei *et al.* 2023). In contrast, limited studies have been performed to predict stress-strain behavior and evaluate mechanical properties of frozen soil (Bakermans and Jamieson 2009, Bayram 2012, Jamshidi *et al.* 2013, Kotilainen *et al.* 2017, Yang *et al.* 2017, Fu *et al.* 2018, Bean *et al.* 2019; Wang *et al.* 2021, Zhu *et al.* 2022), so mainly the constitutive models of frozen soils have been presented. Therefore, in the literature review, in addition, to investigate the prediction of soil behavior and estimation of mechanical parameters of frozen soils, the use of machine learning in the field of AGF studies has also been discussed.

It can be stated that one of the most important and relevant studies in the mentioned area has been done by Nassr *et al*. (2018). They conducted a complete series of triaxial compressive experiments (over 80 samples under different conditions and variables) and investigated frozen SP soil behavior experimentally. Afterward, parameters such as temperature, confining pressure, strain rate, and

*Corresponding author, Ph.D.
E-mail: m.esmaeilifalak@iau-tnb.ac.ir
[a]Assistant Professor

ISSN: 2005-307X (Print), 2092-6219 (Online)

axial strain increment are considered as input variables to modeling the behavior of frozen sand by Evolutionary Polynomial Regression (EPR). It was concluded that the EPR model is able to accurately predict the stress-strain behavior unseen cases (especially frozen SP soils). A sensitivity analysis illustrated that the model developed from raw experimental data is able to extract and effectively represent the underlying mechanics of the behavior of frozen soils.

In an interesting study, frozen soils' mechanical properties have been predicted and optimized via the response surface method (Vahdani *et al.* 2020). The response surface method is a promoting statistical method first to predict then to optimize the mechanical properties (as peak tensile/compressive strength, elasticity modulus) of frozen soils. For this purpose, the input data was prepared from valid references. A comparison between predicted and measured data showed a good agreement with R2 value of 0.887 for the predicted parameters. Besides, it was found that the most influential parameter which strongly influenced the mechanical properties of frozen fine soil is "temperature".

Fei and Yang (2019) conducted a series of unconfined compressive tests on frozen Fairbanks silt at different temperatures (ranging from -0.5 to -10◦C), strain rates, and dry densities (ranging from 1.08 to 1.426 Mg/m3). They then introduce a predictive AI model. It was found that the created model effectively investigates the effects of temperature, strain rate, and dry density on the stress-strain behavior of frozen Fairbanks silt. Eventually, it concluded that the model could be used confidently to simulate the stress-strain behavior of frozen silts similar to Fairbanks silt with R2 of at least 0.98.

Variations of the mechanical properties of natural stones in cold regions due to the freeze-thaw process have been investigated by uniaxial compressive test (Bayram 2012); then a simple linear regression has been used to predict the uniaxial compression strength, Brazilian tensile strength, and modulus of elasticity of the specimens. A comparison between measured and predicted amounts showed that the expanded regression model could be used confidently in the case of uniaxial compression strength of limestone affected by freeze-thaw cycles.

In the cold regions, understanding the behavior of ice alongside frozen soil is of special importance. Kellner *et al.* (2019) have been used machine learning to predict the stress-strain behavior of pure ice. They concluded that the used techniques are suitable and lead to a good agreement between measured and predicted data considering the MCC of 0.782.

Optimization of the freeze tubes arrangement is one of the interesting topics in the field of AGF. Huang *et al.* (2018) first simulated the effect of underground water flow on the active and passive freezing process by coupled thermos-hydro analysis from the standpoint of technical and economical, and then they tried to optimize the position of the freeze pipes against the water flow around circular temporary tunnel support system. The results showed that the proposed optimized arrangement is a well-distribution of freeze pipes, leading to accelerating the active phase, which is economically and temporally desirable.

A simplified model has been developed to predict the tunneling-induced settlement and displacement of the tunnel against the retaining wall's deflection in clayey soil. For this purpose, multiple regression analysis has been used to create a mathematical equation between tunnel displacement and settlements against the effective parameters. The input data for the multiple regression analysis has been generated by finite element analysis. The results showed the highest correlation between measured and predicted values, with 0.921 for R2 in which the simplified model has been validated to be effective in predicting the excavation-induced maximal tunnel displacement (Zhang *et al.* 2020).

A comprehensive review of the technical literature shows that it has not been long since the beginning of the use of neural network techniques in the field of AGF studies, so it can be stated that it still has not reached the full maturity of study because various AI-based methods have not yet been used in the mentioned field to be able to provide a correct and complete comparison between the results of each prediction method using soft computing techniques. So, there is still a great deal to be done. Eventually, in the present study, it is intended to develop more comparative data-mining-based studies to obtain an accurate and reliable technique to predict the Young's modulus of frozen sand.

2. Methodology

In modeling and forecasting investigations, the first and most crucial step is obtaining accurate laboratory results. In such experimental studies, usually each test's conditions (including initial conditions, boundary conditions, peripheral conditions, etc.) are introduced to the model as input parameters and test results as output parameters, and then using these input and output data, the model is trained and tested. Finally, the considered parameter is predicted with acceptable accuracy.

2.1 Testing Equipment and Instrumentation

As described above, experimental tests are required to perform this study. For this purpose, a triaxial compressive test apparatus has been used, which has been developed for frozen soils. The accuracy of the test apparatus and its results have already been validated by reliable studies (Esmaeili-Falak *et al*. 2019), so no further explanation is provided here. In this apparatus, operating temperature range, Cell pressure, and loading speed can be adjusted from +1◦C to -25◦C, 0 kPa to 1500 kPa, and 0.0001 mm/min to 10 mm/min, respectively. A schematic of this apparatus is presented in Fig. 1. The triaxial cell and all its accessories are protected inside a polyurethane insulation chamber to minimize heat loss. Considering the fact that one of the essential parameters of geotechnical design is Young's modulus, in the present study, it is intended to predict the value of E for frozen sandy soils under different variable parameters (T, CP, SR, S, and t). Also, a photo of

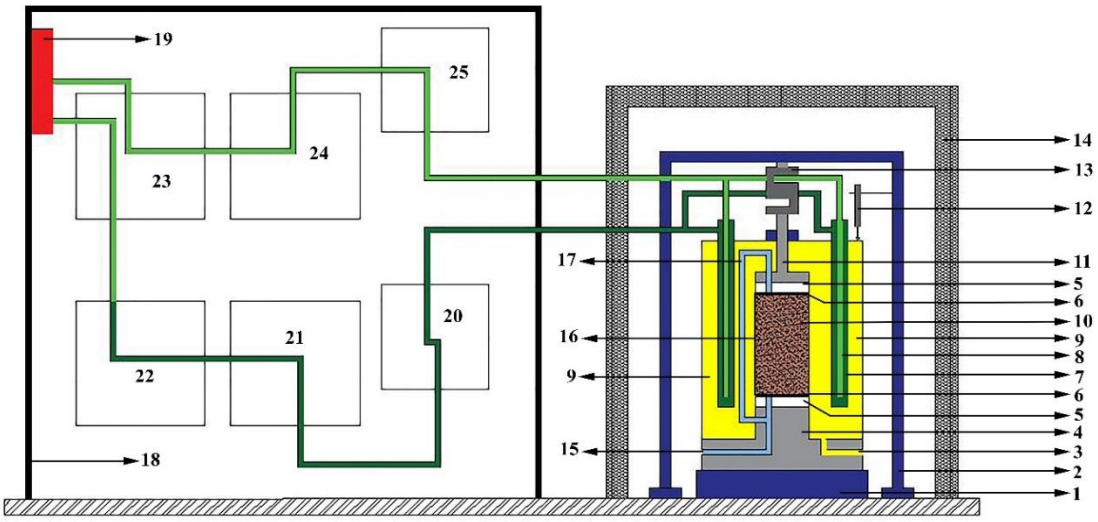

Fig. 1 A schematic of triaxial compressive apparatus for frozen soils: (1) electrical jack (deviatoric stress), (2) rigid chassis, (3) confining pressure measurement, (4) pedestal, (5) thermal isolator, (6) porous disc, (7) outlet pipe, (8) inlet pipe, (9) ethanol (cell pressure liquid), (10) soil specimen, (11) loading piston, (12) LVDT, (13) load-cell, (14) thermal insulation box, (15) pore-pressure and back-pressure measurement, (16) membrane, (17) cap drainage path, (18) refrigeration plant box, (19) cooling fan, (20) pump, (21) evaporator, (22) compressor, (23) cooling pump, (24) condenser, (25) thermostat-thermometer

Fig. 2 A photo of test apparatus and the laboratory

test apparatus and the laboratory circumstance has been illustrated in Fig. 2. Fig. 3 presents the sample results of triaxial test on frozen and unfrozen SP specimens. As can be seen in Fig. 3, Unfrozen SP samples demonstrate strain-hardening behavior while the frozen SP samples illustrate strain-softening behavior. Besides, temperature reduction leads to increase in shear strength and Young's modulus of frozen SP samples. Similarly, increase in loading rate leads to increase in shear strength and Young's modulus of frozen SP samples.

In order to prepare samples of frozen soil, uniform and fine sand (quartz sand) have been used for the triaxial compressive test. The physical properties of the used soil are presented in Table 1. The properties of this sand are similar to Manchester fine sand, and these types of sands are mainly used in most laboratory studies and physical

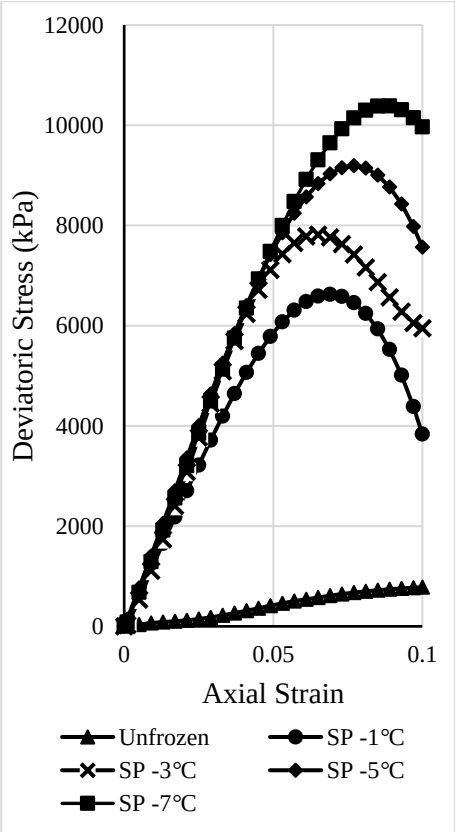

(a) Influence of freezing and temperature decreasing

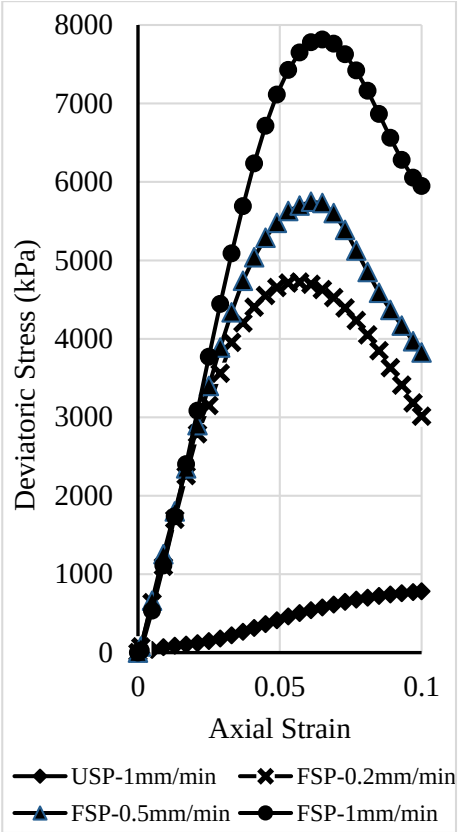

(b) Influence of loading rate

Fig. 3 Samples of experimental triaxial shear test results

Table 1 Physical properties of the soil samples

Parameter	unit	Value
saturated unit weight	kN/m^3	19
water content	%	19.3
water absorption	%	1.99
specific gravity	-	2.72
bulk density	-	1.67
internal friction	°	32
cohesion	kPa	0
classification (according to USCS)	-	SP
grain size range	mm	0.07-0.6

modeling. All samples were prepared in saturation degree of 100% with dimensions of 50 mm in diameter and 100 mm in height. After ensuring complete saturation of the samples, the freezing process continued until reaching the determined temperature. The specimens were then subjected to shear stress (deviatoric stress) under determined Cell pressure and strain rate. After the occurrence of failure and the end of the test, the shear stress diagram against the axial strain is surveyed, and the E is obtained for each test.

2.3 Experimental testing procedure

It is necessary to pay attention to two points in performing these experiments. First, the experiments were performed in unconsolidated undrained conditions, because in practice, due to the low permeability and loading speed of frozen soil, consolidating and draining of that is impossible. Second, to evoke the modeling of the actual project conditions (conditions after the frozen soil body formation), the samples were first frozen and then subjected to Cell pressure. Considering SR, CP, T, t, and S as input variables, Young's Modulus predicted using nine single and hybrid models. A total of 250 triaxial compressive tests on frozen sandy soil samples were conducted. Due to frozen sands' characteristics, unconsolidated undrained freezing soil triaxial tests were performed on all samples. Test results are presented in Table 2. To ensure the accuracy of the results, the experiments were repeated until obtaining a valid result.

Histograms of data sets as Young's Modulus, Cell Pressure, Strain Rate, Temperature, time, and Strain are presented in Fig. 4.

2.3 Experimental testing procedure

It is necessary to pay attention to two points in performing these experiments. First, the experiments were performed in unconsolidated undrained conditions, because in practice, due to the low permeability and loading speed of frozen soil, consolidating and draining of that is impossible. Second, to evoke the modeling of the actual project conditions (conditions after the frozen soil body

Table 2 Statistical characteristics of variables and results

Phase	Index	Inputs					Output
		T	CP	SR	S	t	E
Train data	Min	-11	0.0	0.1	4.1	300	47.637
	Max	-0.500	800	1.5	7.300	3240	160.529
	Average	-3.582	136.885	0.59	5.792	918.098	109.117
	Std. Deviation	2.293	198.334	0.355	0.806	669.741	26.728
Test data	Min	-9.000	0.0	0.1	5	348	49.820
	Max	-0.700	800	1.0	7.5	3000	160.011
	Average	-3.948	202.381	0.733	6.176	803.714	111.490
	Std. Deviation	2.364	225.977	0.354	0.655	695.412	27.613

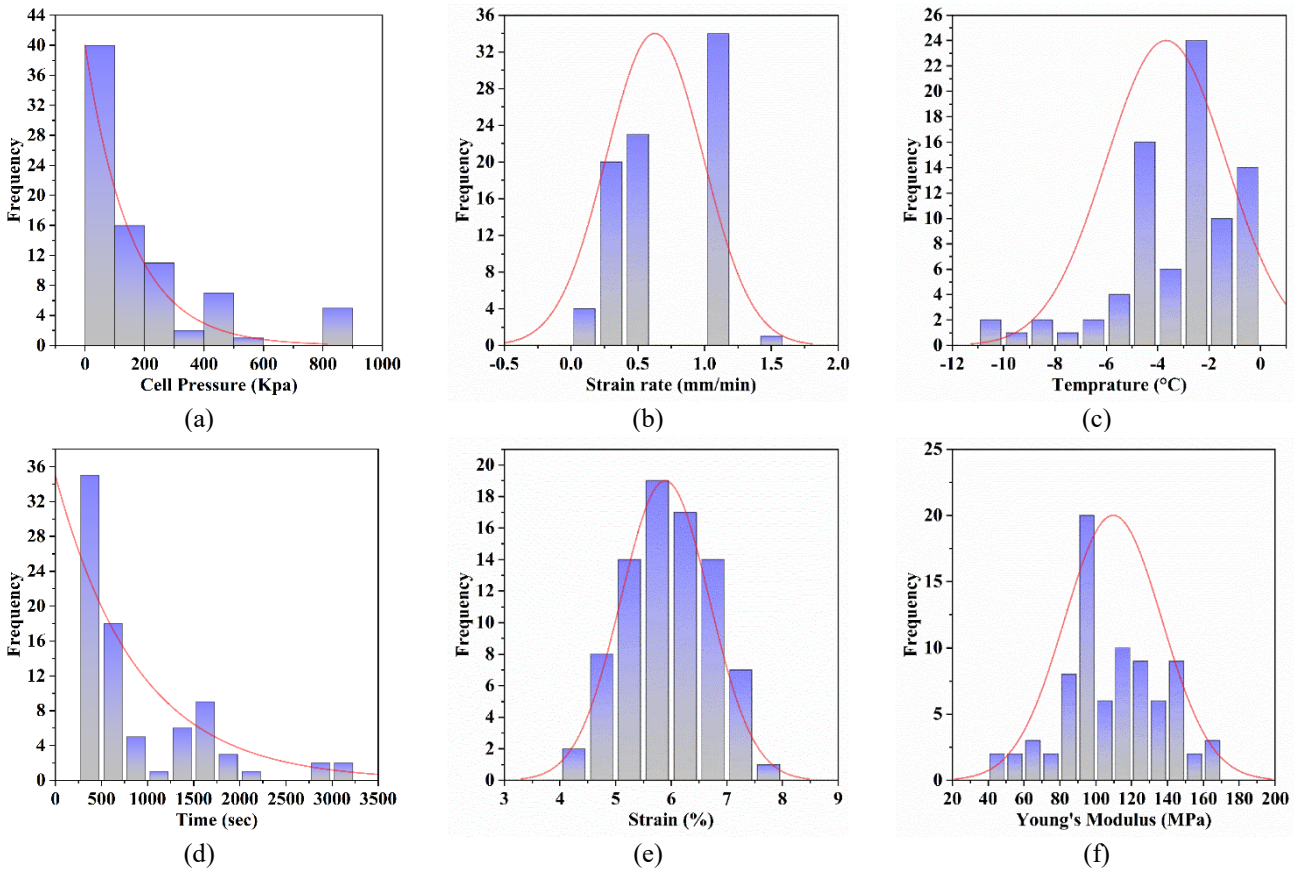

Fig. 4 Histograms of: (a) Cell Pressure, (b) Strain Rate, (C) Temperature, (d) time, (e) Strain and (f) Young's Modulus

formation), the samples were first frozen and then subjected to Cell pressure. Considering SR, CP, T, t, and S as input variables, Young's Modulus predicted using nine single and hybrid models. A total of 250 triaxial compressive tests on frozen sandy soil samples were conducted. Due to frozen sands' characteristics, unconsolidated undrained freezing soil triaxial tests were performed on all samples. Test results are presented in Table 2. To ensure the accuracy of the results, the experiments were repeated until obtaining a valid result. Histograms of data sets as Young's Modulus, Cell Pressure, Strain Rate, Temperature, time, and Strain are presented in Fig. 4.

Fig. 5 shows three-dimensional surface plots of the datasets gained by interpolation using a thin-plate spline. As it can be observed, the relation between E and the input parameters is extraordinarily non-linear and complicated. For instants in Fig. 5(a), the E tends to be high for high CP values and with a peak region of the E for CP at 800 kPa; But E does not have a distinct and regular relationship with S. It can be seen in Figs. 5(b)-5(d) that E also does not have a distinct and regular relationship with t; vis-a-vis maximum values of E occur in lower amounts of T. It also has high values usually ranging approximately 0.5 to 1 mm/min.

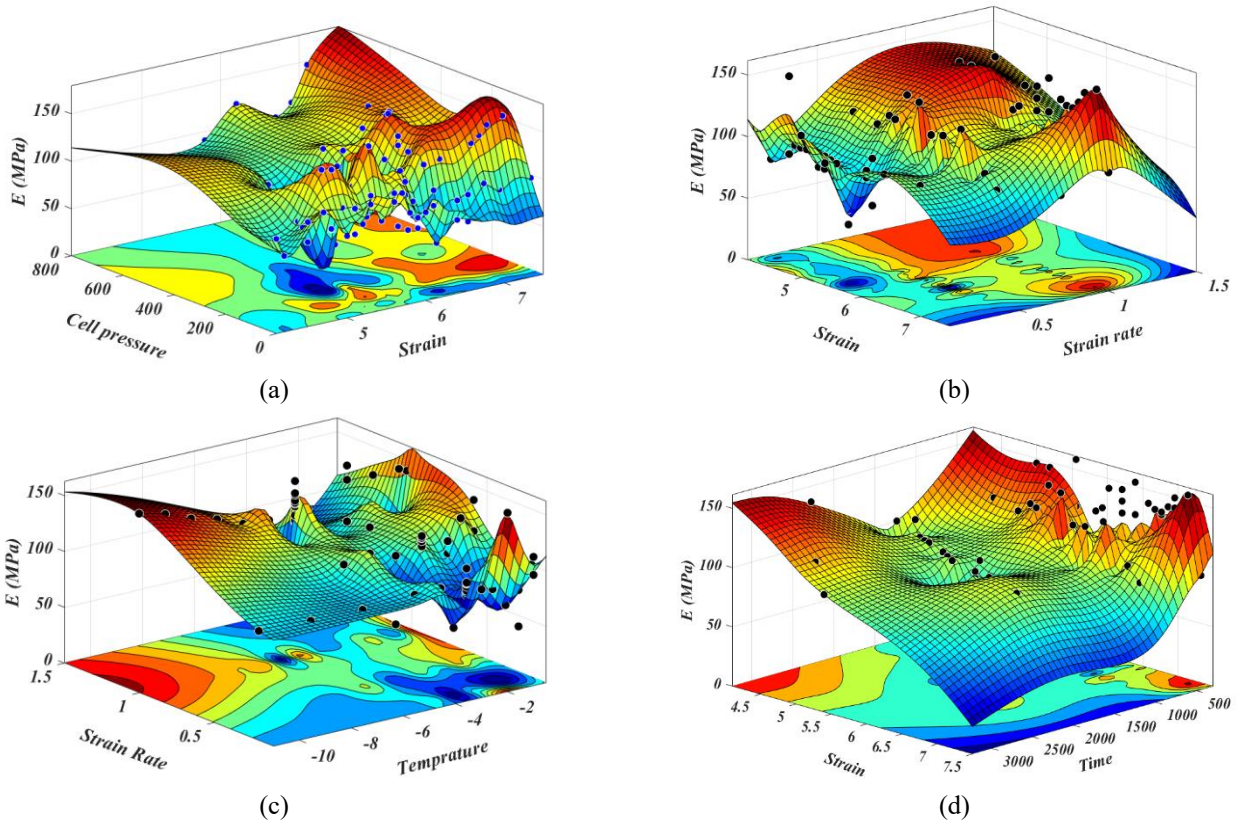

Fig. 5 Surface plots of E versus (a) CP-S, (b) S-SR, (c) SR-T, and (d) S-t

2.4 Parameter setting of data mining models

Due to being time-consumed and containing technical and economic issues of experimental tests, nine single and hybrid models were selected in order to predict the E of the frozen sandy soil samples and compare the results predicted to find the best operation. This research was carried out by investigating the forecasting accuracy of different data mining models, including the tree-based learning algorithms (M5P and RF), rules (M5R), Lazy-learning Algorithms (LWL), Functions (SVR, MLP, and GPR), and Meta classifiers (AR and BAG). The accuracy of the predicted amounts has been investigated by conventional model performance statistical criteria. A list of the regression algorithms with their parameter settings to achieve their highest accuracy in this study is presented in Table 3.

The regression tree models are more superficial than that of the classification tree approaches. A stepwise optimal tree structure in the least square regression has been used to have come into being in 1963 proposed by Morgan and Sonquist to automatic interaction detection programming. Sonquist and Morgan developed it in 1964, Sonquist in 1970, Sonquist *et al.* (1973), and finally, it was perfect in 1980 by Van Eck. Some of the AI-based individual studies illustrated that their research provides more accurate results than that of regression tree models; however, regression tree models are faster and easier to interpret (Omran *et al*. 2016). In another study, the modulus of elasticity and shear strength of frozen sand have been predicted by regression tree models and compared them with IA-based method as ANN, ANFIS, and SVM which presented by Esmaeili-Falak *et al*. (2019). Therefore, it is necessary to expand regression tree models in other civil engineering scopes, especially concrete technology science. An expanded graphical diagram of the programming of the present study is illustrated in Fig. 6.

2.5.1 Tree-based learning algorithms

2.5.1.1 M5P

M5 algorithm is modified to create a tree regression model using empirical data named M5P (Quinlan 1992). It has an approach in which a model tree is applied for scalar predictions, so at each leaf underlay of each branch, it stores a linear regression model which predicts the leaf relevant class values. Pursuant to the determined attributed data set, it splits into disparate contributions. Generally, Standard Deviation Reduction, which is estimated using Eq. (1), is exerted as a measure that specifies the best feature for dividing the data set at each node. This procedure ended almost at minimal variations in class value. Then sharp discontinuities among the neighbor linear models smoothen by pruned back of the tree. Considering the following equation, this technique exceptionally decreases the expected errors in the node.

$$SDR = sd(T) - \sum_{i} \frac{|T_i|}{|T|} \times sd(T_i) \quad (1)$$

where sd, T and Ti are the standard deviation, a set of

Table 3 Chose parameter context to assess the highest accuracy of the testing techniques

Categories	Method	Name of parameter	Selected value
Functions	SVR	Kernel of the choice	RBF
		Gamma value	0.01
	MLP	Node number for first hidden layer	15
		Node number for second hidden layer	8
		Learning rate	0.1
		Momentum	0.25
		Training time	10000
		Validation threshold	20
	GPR	Kernel of the choice	RBF
		Gamma value	0.01
		Level of Gaussian noise	0.01
Lazy-learning algorithms	LWL	Base classifier	Gaussian process
		Kernel of the choice	RBF
		Gamma value	0.01
		Level of Gaussian noise	0.01
Tree-based learning algorithms	M5P	Minimum number of instances	4
	RF	Bag size percentage	100
		Number of execution slots	1
		The number of trees	80
Meta classifiers	AR	Base classifier	Gaussian process
		Number of iterations	50
		Shrinkage rate	1
		Level of Gaussian noise	0.03
		Kernel of the choice	RBF
		Gamma value	0.01
	BAG	Base classifier	Gaussian process
		Number of iterations	80
		BAG size percentage	100
		Level of Gaussian noise	0.007
		Kernel of the choice	RBF
		Gamma value	0.01
Rules classifiers	M5R	Minimum number of instances	5

examples that each note, and the node division's outcomes according to the attributes, respectively.

2.5.1.2 Random forest

RF is a user-friendly Data-mining algorithm that frequently constructs excellent results, even without hyper-parameter tuning (Breiman 2001). Due to simplicity and diversity RF is one of the most used algorithms (for the ability of classification and regression). RF is a monitored learning machine. The "forest" it builds is an accumulation of decision trees, which normally trained with the "bagging" technique. The conventional concept of the BAG technique is that a blending of learning models thoroughly raises the result. RF creates various decision trees and combines them to achieve a more precise and stable prediction. One significant benefit of RF is that it can be utilized for both classification and regression issues, which construct the mostly of current data mining techniques. (Misra and Li 2019). The training phases of RF are as bellows: (a) Based on the dataset, draw an example that is selected accidentally with replacement. (b) With aid of the bootstrap sample, derive a tree with these corrections: for every knot, choose the best-randomized subset of m try signifiers (i.e., the number of predictors tried per each knot). M try here has the role of tuning a parameter in the RF technique. The tree is generated to its maximum size without tuning it. (c) Stage (b) is iterated until the user-manual numbers of trees (N-tree) are grown on the basis of the bootstrap instance of observations. The final prediction values are determined by combining all individual tree outcomes. After growing K trees {Tk(x)}, the regression explanatory variables in RF are stated by the following formulation

$$f(x) = (\sum_{K=1}^{K} T_k(x))/K \quad (2)$$

A new training set for each built RF regression tree is derived by replacing the main calibrating phase. Thus, after stablishing a regression tree each time, through the application of a randomized training sample, the out-of-bag sample is used to verify the accuracy (Eq. (3)).

$$GI(t_{X(xi)}) = 1 - \sum_{j=1}^{m} f(t_{X(xi),j})^2 \quad (3)$$

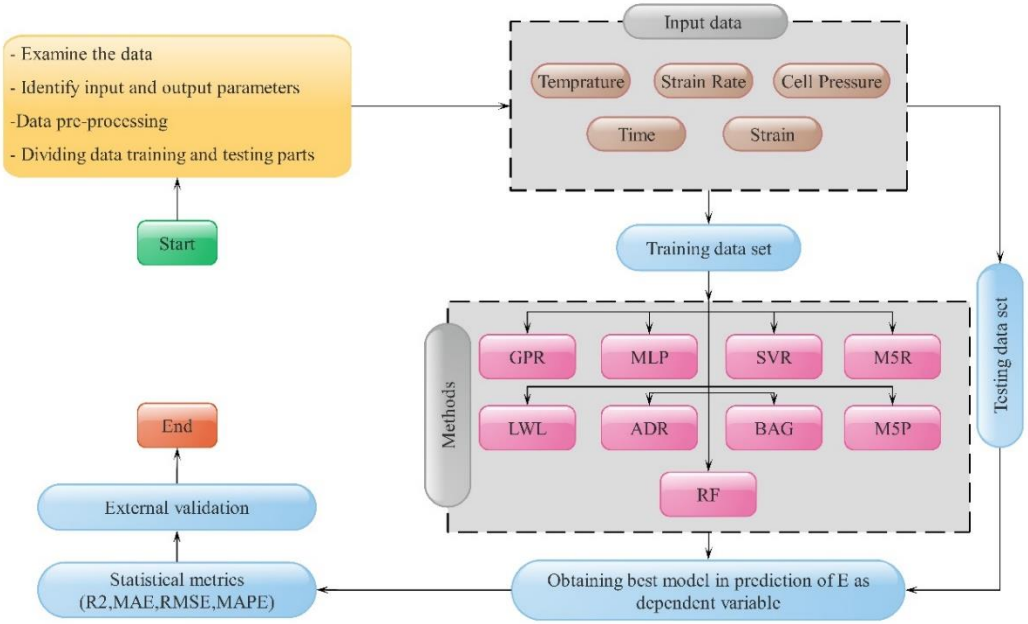

Fig. 6 Graphical diagram of programming of the present study

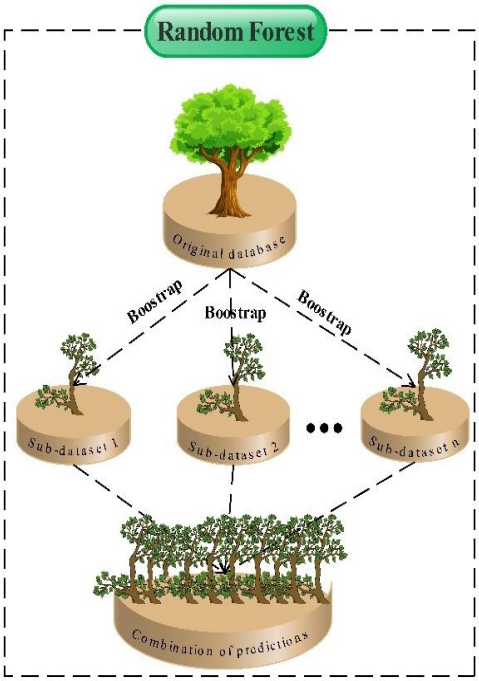

Fig. 7 Standard architecture of RF algorithm

The verification specifications enhance the soundness of RFs due to using independent test data. The RF model (Fig. 7) is a practical technique for classification and regression purposes.

2.5.2 Rules

2.5.2.1 M5P

A model tree is employed to complete the train of the dataset, which leads to a pruned learned tree (Holmes *et al*. 1999). Then using the heuristic calculations, the best leaf at each branch is constructed as a rule, and threw away the remained tree and all covered cases by the rule are ignored from the dataset. The process is employed iteratively to the residual cases and finishes when one or more rules cover all cases. Instead of creating a single rule, as it is done usually, a full model tree is created at each stage and makes its "best" leaf into a rule. Despite the PART algorithm (Frank and Witten 1998), which uses the identical mechanism for the categorical prediction, M5-Rule construct complete trees in lieu of partially explored trees. Building partial trees leads to greater computational performance and does not influence the resulting rules' size and accuracy. Because the tree-shape which a rule is created is discarded at each step, smoothing for laws would have to be done as a post-processing step after the full set of rules has been generated. This procedure is more complicated than that of smoothing technique trees-it would include specifying the boundaries between laws and then positioning linear models to smooth over them.

2.5.3 Lazy-learning algorithms

2.5.3.1 LWL

LWL is a type of lazy acquisition and memory-based acquisition and localizes on LWL algorithm (Atkeson *et al*. 1997). The study considers interval functions, smoothing variables, weighting functions, local model textures, regularization of the assessments and bias, evaluating predictions, investigating noisy data and outliers, amending the quality of predictions by tuning fit variables, interposition between old and new data, performing LWL accurately, and applications utilizations of LWL. A companion paper evaluates how LWL can be applied in robot acquisition and regulate. For a standard regression

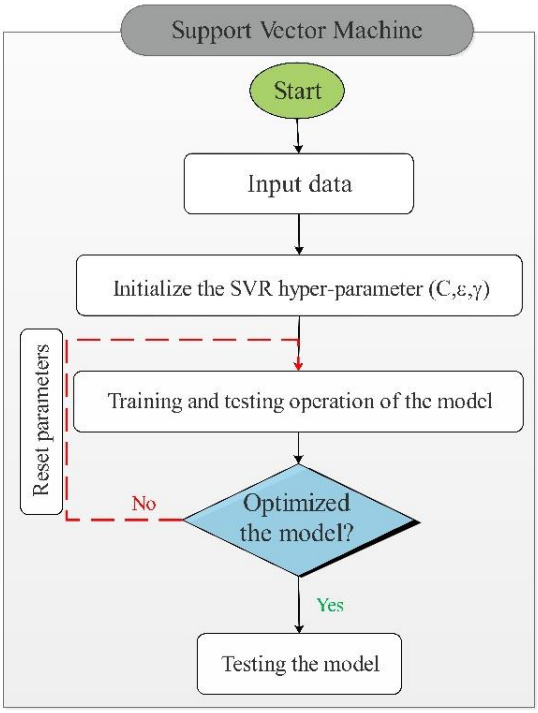

Fig. 8 General layout of SVR Technique

model like y=f(x)+ϵ where f(x) and ϵ are continuous function and noise, respectively. The basis cost function of LWL is as Eq. (4)

$$J = 0.5\sum_{i=1}^{n} \omega_i(x_q)(y_i - x_i\beta_q)^2 \quad (4)$$

Where, labeled training data is D= $\{(x_i, y_i)|i=1, 2, \ldots, n\}$ that each data point x_i belongs to a corresponding output value y_i; a point of interest is x_p (also called query point), that is the position where we want a prediction $\hat{y}_q$; weights ω_i describe the relevance of the corresponding training set (x_i , y_i) for the current prediction. They are dependent on the query point and are computed by a weighting function; and regression coefficient β_q of our linear model, which we want to obtain for making the prediction.

2.5.4 Functions

2.5.4.1 SVR

Constructive risk minimalization presumption inferred SVM is a statistical learning algorithm that minimizes the training machine's experimental risk and confidence interval, consequently leading to a reasonable capacity for generalization (Deka 2014). Cortes and Vapnik (1995) expanded the theory of the SVM in 1995. Considering a series of training parameters$\{(x_i + d_i)\}_i^N$, where x_i, d_i, and N are the input vector, eligible quantity, and the whole issues of data templates, respectively, the SVM's regression function is formularized as (Eq. (5))

$$f(x) = \omega_i.\varphi_i(x) + b \quad (5)$$

where, "b" is the bias, ω_i is a weight vector, and φ_i demonstrates a non-linear transition function that schemes the input vectors into a multi-dimensional properties space. Theoretically, a plain linear regression can accompany by the wrapped non-linear regression of the input area. Fig. 8 represents a typical SVR layout.

Dissolving this outstanding optimization issue with an e-insensitivity loss function, Vapnik (2013) dissolved Eqs. (6) and (7) as

$$\text{minimize: } 0.5\|\omega\|^2 + C(\sum_{i=1}^{N}(\xi_i + \xi_i^*)) \quad (6)$$

$$\text{Subject to: } \begin{cases} [\omega_i \times \emptyset(x_i)] + b_i - d_i \le \epsilon + \xi_i^*, & i = 1, 2, \cdots, N \\ d_i - [\omega_i * \emptyset(x_i)] - b_i \le \epsilon + \xi_i, & i = 1, 2, \cdots, N \\ \xi_i, \xi_i^*, & i = 1, 2, 3, \cdots, N \end{cases} \quad (7)$$

C: a positive trade off variable that specifies the degree of the experimental error in the optimization issue

ξ_i , ξ_i^* : slack parameters that assess errors of training by the loss function over the tolerance of error ξ_i

2.5.4.2 MLP

A multilayer perceptron is a class of feedforward artificial neural networks. MLP is utilized mistily, occasionally loosely to any feedforward artificial neural network, sometimes rigorously relegating to networks made of multiple layers of perceptron (with threshold activation). MLPs are occasionally commonly relegating to as "vanilla" neural networks, especially when they have a single hidden layer. An MLP contains at least three layers of knots: one input, one hidden layer, and one output layer. Unless the input knots, each knot is a neuron that utilizes a nonlinear activation function. MLP uses a controlled learning

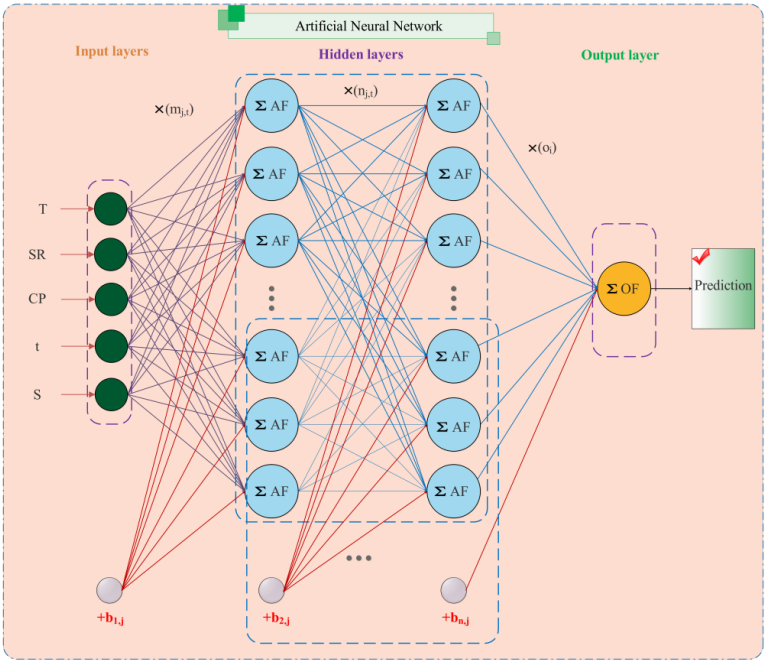

Fig. 9 Created ANN model for the present study

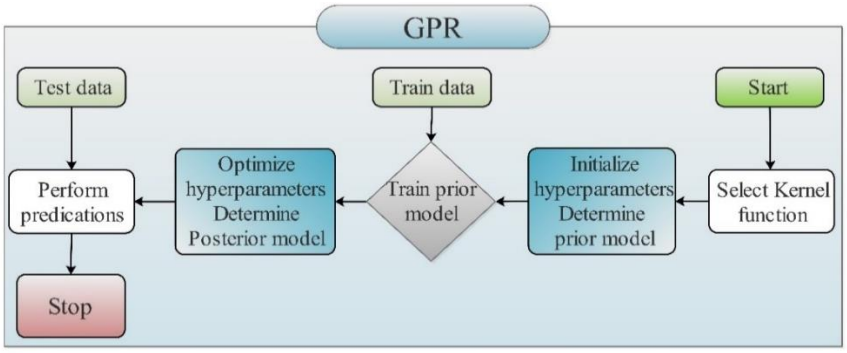

Fig. 10 General layout of GPR

approach named backpropagation to train the data. The multiple layers of the model and non-linear activation differ MLP from a linear perceptron. It can determine data that is not linearly detachable. The term "multilayer perceptron" does not relegate to an individual perceptron that has multiple layers. Instead, it includes lots of perceptrons that are arranged into layers. A choice is the "MLP network." Moreover, MLP "perceptron" is not perceptron in the tough feasible concept.

Genuine perceptron is regularly a particular instance of artificial neurons that utilize a threshold activation function like the Heaviside stage function. MLP perceptron can utilize optional activation functions. A genuine perceptron carries out dual grading, and an MLP neuron is free to either conduct grading or regression, depending upon its activation function. After that, the phrase "multilayer perceptron" was used without respect to the essence of the knots/layers, which can be contained desirable defined artificial neurons and not perceptron clearly. This interpretation avoids the loosening of the definition of "perceptron" to mean an artificial neuron generally. Double historical conventional activation functions are both sigmoid and are presented as Eq. (8)

$$y(v_i) = tanh(v_i)\ \&\ y(v_i) = (1 + e^{-v_i})^{-1} \quad (8)$$

The equation for each MLP layer is shown as Eq. (9)

$$Y_j = F(\sum W_{ij}X_i - \theta_j) \quad (9)$$

in which $Y_i, W_{ij}, \theta_j, and\ F(x)$ are the output of neuron j, the connection weight from neuron i to neuron j, the signal produced for neuron i, the bias accompanied by the neuron j and the different activation functions, respectively. An instance of ANN model with seven input parameters is shown in Fig. 9.

2.5.4.3 GPR

GPR (Fig. 10) is a Bayesian nonparametric technique (i.e., not limited by a functional form) which extensively used in data mining of different systems (Chen *et al*. 2007), thus instead of computing the feasibility distribution of

variables of an especial function, GPR computes the probability distribution over all allowable functions that fit the data (Wang and Chen 2015). There are multiple libraries for effective performance of GPR (e.g., scikit-learn, Gpytorch, GPy). In GPR, it is first assumed a Gaussian process prior, which can be specified using a mean function, m(x), and covariance function, k (x, x')

$$f(x) \sim GP(m(x), k(x, x')) \tag{10}$$

A Gaussian process is specifically similar to an infinite-dimensional multivariate Gaussian distribution, where any complex of the dataset tags is joint Gaussian distributed. Within this GP former, we can combine prior learning about the space of functions through the choice of the mean and covariance functions. We can also easily combine independently, accurately distributed (i.i.d) Gaussian noise, $\epsilon \sim N(0, \sigma^2)$, to the labels by pluralization the tag and noise distributions

$$y \sim GP(m(x), k(x, x') + \delta_{ij}\sigma_n^2) \tag{11}$$

2.5.5 Meta classifiers

2.5.5.1 Additive regression

The AR approach (Friedman 2001) is a specialized AR tree in which the constitutive learner h(x;a) is a J-terminal node regression or a classification tree (Friedman *et al*. 2003). AR models use an algorithm in which each iteration is named m, a new regression model $T_m\left(x; \{R_{jm}\}_1^J\right)$ is made to separate the x-space toward J discontinuity area $\{R_{jm}\}_{j=1}^J$ and predict a new individual constant amount in any of them. It is worth mentioning that the AR model enhances the efficiency of the regression tree models' low accuracy using the stochastic AR technique.

AR is typically used with tree-based learning algorithms of a stable extent as a root learners. For this specific instance, Friedman suggests a correction to the AR technique, which enhances each base learner's quality of fit. Generic AR at the mth stage would fit a decision tree hm(x) to pseudo-residual. Let Jm be the number of its leaves. The tree partitions the input area into Jm decomposed spaces R1m, Rjm and forecasts a stable amount in each space. Using the index annotation, the output of hm(x) for input x can be written as the Eq. (12)

$$h_m(x) = \sum_{j=1}^{j_m} b_{jm} 1_{R_{jm}}(x) \tag{12}$$

Friedman suggests to correct these models so that it selects a discrete optimized amount γ_{jm} for each of the tree's spaces instead of a lone γ_m for the complete tree. He calls the improved model "TreeBoost." The factors b_{jm} from the tree-fitting process can be then commonly threw away, and the algorithm update principle develops into

$$\begin{aligned} F_m(x) &= F_{m-1}(x) + \sum_{j=1}^{J_m} \gamma_{jm} 1_{R_{jm}}(x), \gamma_{jm} \\ &= \underset{\gamma}{argmin} \sum_{x_i \in R_{jm}} L(y_i, F_{m-1}(x_i) + \gamma) \end{aligned} \tag{13}$$

2.5.5.2 Bagging predictors

Breiman (1996) explained the BAG model as an approach to produce multiple versions of a predictor, applying these to obtain a more accurate predictor. The mean density over the versions while an output predicted leads to a multiplicity sentence predicting a category. Providing the bootstrap replicates of the learning date set and applying as new learning sets organize the multiple versions. The output of trained and tested data sets by classification, regression trees, and linear regression showed that the BAG model presented far more accurate predictions. In regression predictor, if distributing the input data leads to the predictions, thereupon the BAG approach can be used reliability. BAG technique implementation is as below:

(a) N training subset are produced with:

- $p \leq n$ bootstrap data instances were drawn, with or without replacement, from the original training set of n data samples;
- $p \leq m$ ascribes from the principal m dimensions of the dataset;

(b) A forecasting approach hT (x) is trained on each bootstrap T=1, …, N. This conduces to the ultimate ensemble technique H(x)={hT(x), T=1, …, N};

(c) To utilize the ensemble technique H(x) is based on a complex of the forecasters created by all model hT(x).

In a classification issue, the majority vote or the average stage score can be used. The majority vote takes the category anticipated by most models hT (x,ci) as the final class. The average category score takes the class anticipated by the highest average score computed on all techniques hT (x, ci):

$$c_i = argmax_i\{\frac{1}{N}\sum_{T=1}^{N} \mathrm{h_T}(\mathrm{x}, \mathrm{c}_i)\} \tag{14}$$

In a numeral anticipation issue, the average amount computed on all techniques hT(x) is utilized

$$y_p = \frac{1}{N}\sum_{T=1}^{N} \mathrm{h_T}(x) \tag{15}$$

2.6 Model performance assessment criteria

For evaluating the efficiency of the predicted amount of E of frozen sand samples (in both trained and tested phases) versus the measured amounts, six criteria were used including the root mean squared error (RMSE), the mean absolute error (MAE), the squared coefficient of determination (R^2), Mean Absolute Percentage Error (MAPE), performance index (PI), and OBJ according to the Eqs. (16) to (21), where y_P and t_P present the predicted and measured values of the P^th pattern, and $\bar{t}$ and $\bar{y}$ show the averages of the measured and predicted values, respectively. RMSE and MAE's lower values and the higher values of R^2 represent the models' higher performance.

$$RMSE = \sqrt{\frac{1}{P}\sum_{p=1}^{P}(y_p - t_p)^2} \tag{16}$$

$$MAE = \frac{1}{P}\sum_{p=1}^{P}|y_p - t_p| \quad (17)$$

$$R^2 = \left(\frac{\sum_{p=1}^{P}(t_P - \bar{t})(y_P - \bar{y})}{\sqrt{\left[\sum_{p=1}^{P}(t_P - \bar{t})^2\right]\left[\sum_{p=1}^{P}(y_P - \bar{y})^2\right]}}\right)^2 \quad (18)$$

$$MAPE = \frac{1}{P}\sum_{p=1}^{P}\left|\frac{t_P - y_P}{t_P}\right| \quad (19)$$

$$PI = \frac{1}{|\bar{t}|}\frac{RMSE}{\sqrt{R^2}+1} \quad (20)$$

$$OBJ = \frac{n_{train}}{P}\left(\frac{RMSE_{train} + MAE_{train}}{R^2{}_{train} + 1}\right) + \frac{n_{test}}{P}\left(\frac{RMSE_{test} + MAE_{test}}{R^2{}_{test} + 1}\right) \quad (21)$$

Compared with some of the state-of-the-art models, regression tree models may have lower prediction accuracy but usually perform faster and are easier to interpret. This research examined four commonly used regression tree models as subsequently described.

3. Results and discussions

Young's modulus is one of the most important parameters in designing artificial ground freezing projects. For obtaining E, 250 triaxial compressive tests (considering the validation iteration) have been done on frozen sand samples in the present. Using the results of these experiments T, CP, SR, S and t considered as input parameters to forecast the E. 75% and 25% of the total results are given as training and testing data, respectively.

3.1 Comparison of the predicted results

The experimental measured E of frozen sand versus the predicted values generally has a good agreement in all models, as shown in Figs. 11-15. Performance assessment criteria of all models and their final ranking are presented in Tables 4 and 5. According to the prediction of training data, the MLP and GPR techniques have the best and the worst performance in predicting the E of frozen sand among all nine models, respectively, considering the final ranking (Table 4); also, the SVR model's accuracy of prediction is reasonable. Reflecting the R2 and RMSE in function models, MLP, SVR, and GPR have the best, acceptable, and the worst accuracy in forecasting the training data, respectively. Considering the MAE in function models, MLP, SVR, and GPR have the best, very well, and the worst outputs in forecasting the training data. Also reflecting the MAPE in function models MLP, SVR, and GPR have excellent, very well and weak outputs in predicting the training data. Regarding the prediction of training data in the category of Function models (SVR, MLP, and GPR), according to Table 4, the MLP technique has the best performance in predicting the E of frozen sand, with R2, RMSE, MAE, and MAPE equal to 0.9973, 1.7533, 1.3322 and 0.000098, respectively. In contrast, the lowest rank belongs to GPR, either among all models or function models, at R2, RMSE, MAE, and MAPE, 0.8788 (14% lower than MLP), 9.3517 (81% greater than MLP), 6.9514 (81% greater than MLP), and 0.00056 (83% greater than MLP), respectively. In this category, the SVR's accuracy is between the two mentioned models, belongs the R2, RMSE, MAE, and MAPE of 0.9339, 7.1469, 4.0245, and 0.000113, respectively. Additionally, regarding R2, RMSE, MAE, and MAPE indexes in function models, MLP, SVR, and GPR have the best, reasonable, and the worst outputs, respectively. All in all, according to the total ranking score system, the MLP model has the highest rank, the second rank belongs to the SVR model, and the last rank is for GPR.

Considering tree-based learning algorithms in forecasting the training data, RF's accuracy is much better than that of the M5P so that the R2, RMSE, MAE, and MAPE of RF are 0.9814, 3.9213, 2.6617, and 0.000263, respectively; while the mentioned indexes for the M5P are 0.9372, 6.8576, 5.4209 and 0.000638, respectively. By assessing the indexes of training data, the forecasting precision of M5R and LWL is well with R2 of 0.9514 and 0.9338. Due to the relatively poor performance of the GPR compared to other models in training data, AR-GPR and BAG-GPR were employed to improve their performance by hybridizing. Both hybrid models improved GPR-performance, but the degree of improvement of AR is much higher than BAG-GPR, so that AR-GPR and BAG have improved the GPR's ranking from 9 to 3 and 8, respectively. Hybridization increases R2 of GPR from 0.8788 to 0.9555 (for AR-GPR) and 0.9041 (for BAG-GPR) for training data that have high accuracy.

Nevertheless, the models' ranking is entirely different based on the accuracy of prediction of E in testing data (Table 5); BAG and AR have the best performance while RF has the lowest prediction accuracy. The best predictions considering the R2, RMSE, MAE, and MAPE are associated with BAG-GPR, BAG-GPR, AR-GPR, and AR-GPR, respectively, while the worst forecasting accuracy is related to RF based on all of the model performance assessment criteria. In general, all models' prediction accuracy based on testing data is less than that of training data. However, the predicted values are acceptable, and they can help us with economic designing in artificial ground freezing projects. Hybridization is more efficient based on testing data predictions, and it can be concluded that it is more effective at lower forecasting accuracy in models.

Fig. 11 shows the squared correlation coefficient for the Function models as GPR, MLP, and SVR. It can be seen that the accuracy of the predictions based on training data is much more than testing data, which is also consistent with previous studies. According to Fig. 11, based on the training data, the accuracy of predictions in MLP is more than SVR and in SVR is more than GPR, while based on the testing data, the accuracy of predictions in GPR is more than SVR and in SVR is more than MLP. All of the predicted values have a reasonable agreement with the experimentally

Table 4 Comparison of the prediction accuracy using different models for training data

Predicting technique	Training phase (Ranking score)						
	R2	RMSE	MAE	MAPE	PI	Total Ranking Score	Final Ranking
GPR	0.8788 (1)	9.3517 (1)	6.9514 (1)	0.00056 (3)	0.391 (1)	7	8
MLP	0.9973 (9)	1.7533 (9)	1.3322 (9)	0.000098 (8)	0.008 (9)	44	1
SVR	0.9339 (4)	7.1469 (3)	4.0245 (7)	0.000113 (7)	0.028 (5)	26	4
LWL	0.9338 (3)	7.0783 (4)	5.3262 (4)	0.000388 (4)	0.033 (3)	18	6
M5P	0.9372 (5)	6.8576 (5)	5.4209 (3)	0.000638 (1)	0.0319 (4)	18	6
M5R	0.9514 (6)	5.9879 (6)	4.7375 (5)	0.000635 (2)	0.0278 (6)	25	5
RF	0.9814 (8)	3.9213 (8)	2.6617 (8)	0.000263 (6)	0.0181 (8)	38	2
AR-GPR	0.9555 (7)	5.6527 (7)	4.1284 (6)	0.000048 (9)	0.0262 (7)	36	3
BAG-GPR	0.9041 (2)	8.2967 (2)	6.1313 (2)	0.00033 (5)	0.0353 (2)	13	7

Table 5 Comparison of the prediction accuracy using different models for testing data

Predicting technique	Testing phase (Ranking score)						
	R2	RMSE	MAE	MAPE	PI	Total Ranking Score	Final Ranking
GPR	0.8538 (8)	10.9445 (7)	8.4866 (4)	0.0047 (5)	0.051 (8)	32	3
MLP	0.8134 (2)	12.1263 (3)	8.5149 (3)	0.0044 (6)	0.0572 (4)	18	6
SVR	0.8496 (6)	11.7025 (6)	8.3446 (5)	0.0036 (8)	0.0546 (7)	32	3
LWL	0.8502 (7)	10.9242 (8)	8.1542 (6)	0.0047 (5)	0.051 (8)	34	2
M5P	0.8335 (5)	12.1791 (2)	8.8197 (2)	0.0047 (5)	0.0571 (5)	19	5
M5R	0.8306 (4)	11.8645 (4)	8.126 (7)	0.0047 (5)	0.0557 (6)	26	4
RF	0.8006 (1)	13.2762 (1)	9.2686 (1)	0.0067 (1)	0.0628 (1)	5	7
AR-GPR	0.825 (3)	11.8456 (5)	7.8247 (9)	0.0029 (9)	0.0557 (6)	32	3
BAG-GPR	0.8546 (9)	10.7332 (9)	8.0054 (8)	0.004 (7)	0.05 (9)	42	1

Table 6 OBJ values

Predicting technique	GPR	MLP	SVR	LWL	M5P	M5R	RF	AR-GPR	BAG-GPR
OBJ	9.1395	**4.0643**	7.073	7.4126	7.6481	6.8853	5.6781	6.4753	8.2244

measured amounts in both training and testing data.

Fig. 12 shows the squared correlation coefficient for tree-based learning algorithms as M5P and RF models. According to Fig. 12, based on the training data, the accuracy of RF predictions is more than M5P, while based on the testing data, the accuracy of predictions in M5P is more than RF. All of the predictions have good agreement with the experimentally measured values in both training and testing data.

Fig. 13 shows the squared correlation coefficient for the M5R model. Considering the final ranking of the model's accuracy based on training (Table 4) and testing (Table 5) data, the rank of M5R is 4 and 6, respectively. The values of R2, RMSE, MAE, and MAPE of M5R based on training data are 0.9514, 5.9879, 4.7375, and 0.000635, respectively, while the mentioned indexes based on the testing data for the M5R model are 0.8306, 11.8645, 8.126, and 0.0047, respectively.

Fig. 14 shows E's predicted values against the measured one based on both training and testing data for the Lazy-learning LWL Algorithm. Considering the final ranking of the model's accuracy based on training (Table 4) and testing (Table 5) data, the rank of LWL is 6 and 2, respectively. The values of R2, RMSE, MAE, and MAPE of LWL based on training data are 0.9338, 7.0783, 5.3262, and 0.000388, respectively; while the mentioned indexes based on the testing data for the LWL model are 0.8502, 10.9242, 8.1542, and 0.0047, respectively. Surprisingly it can be seen that the LWL model has an iconoclastic behavior based on comparing the final ranking between accuracies based on training and testing data, so that, it has excellent operation based on testing data.

Fig. 15 shows E's predicted values against the measured one based on both training and testing data for Hybrid Meta classifier models as AR-GPR and BAG-GPR models. The results show that coupling both AR-GPR and BAG-GPR models generally improves the GPR single model's performance. According to Fig. 15, based on the training data, the accuracy of predictions in AR-GPR is more than BAG-GPR, while based on the testing data, the accuracy of predictions in BAG-GPR is more than AR-GPR. All of the predictions have excellent agreement with the experimentally measured values, especially for the testing data.

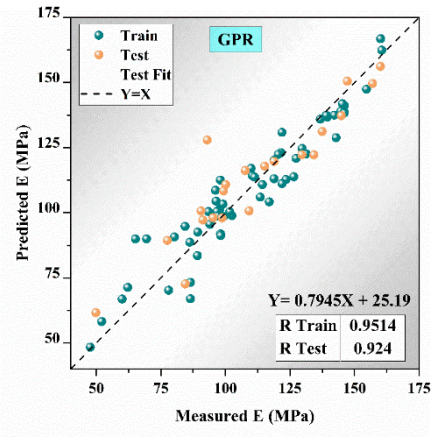

(a)

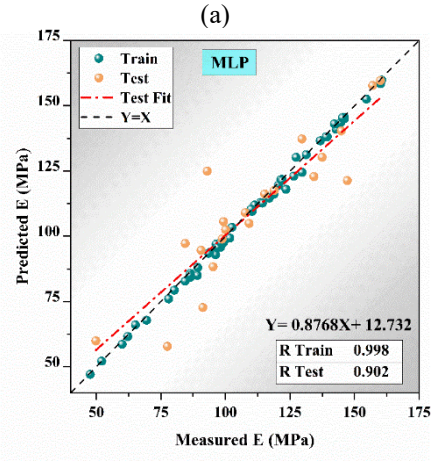

(b)

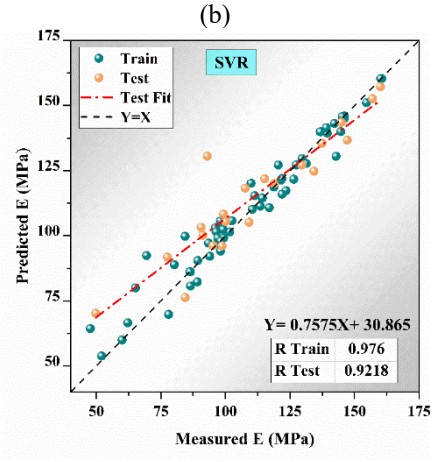

(c)

Fig. 11 The squared correlation coefficient for the Function models: (a) GPR, (b) MLP, and (c) SVR

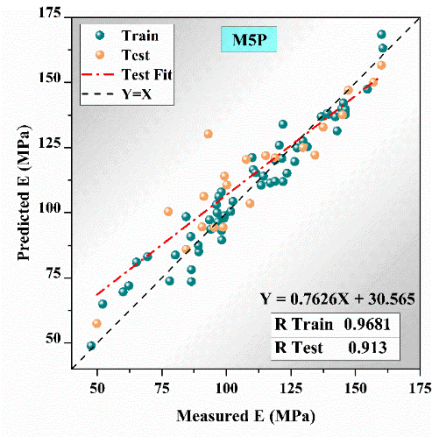

(a)

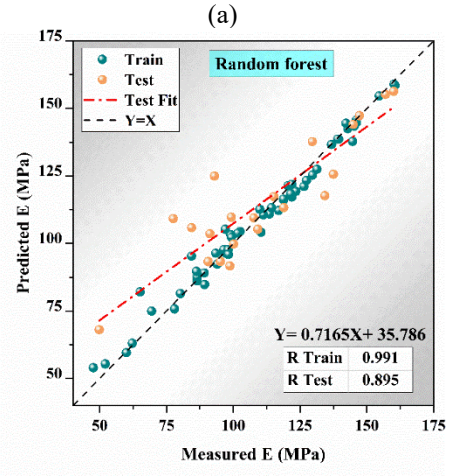

(b)

Fig. 12 The squared correlation coefficient for tree-based learning algorithms: (a) M5P and (b) RF

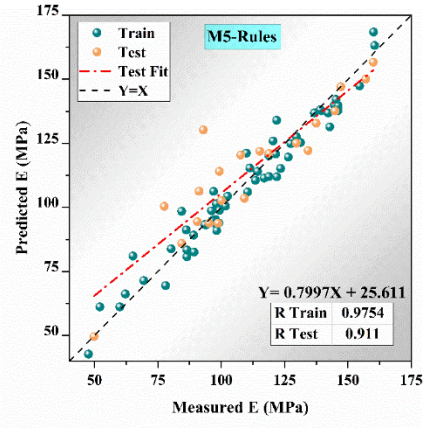

Fig. 13 The squared correlation coefficient for M5R model

The results of the performance assessment of the implemented models are illustrated in Figs. 16 to 24, showing a graphical comparison between the magnitude of errors for both training and testing data, as well as the normal distribution of the errors. According to these figures, it is evident that the errors of both training and testing data are Scattered and irregular for all nine single and hybrid models.

Generally, the errors of the training data are lower than that of the testing data. As shown in Figs. 16 to 24, the most negligible errors are related to MLP, RF, AR-GPR, and SVR models in predicting the training data. The best case for testing data prediction errors comes from hybrid BAG-GPR, hybrid AR-GPR, LWL, and SVR models. According to the Figs. 16 to 24, the highest amount of error for both training and testing data prediction can be seen in GPR and RF models, respectively. Examination of typical distribution diagrams also shows that the models' best behavior is coming from hybrid BAG-GPR, hybrid AR-GPR models.

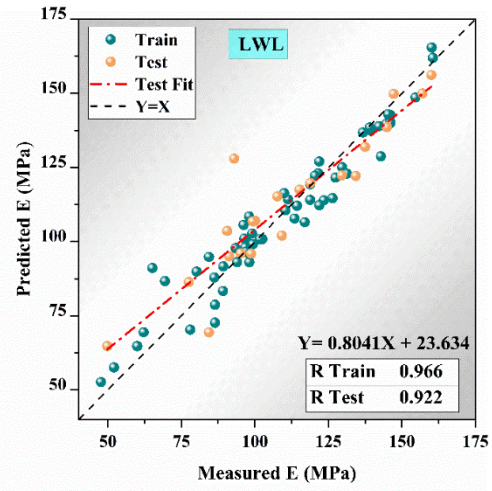

Fig. 14 The squared correlation coefficient for Lazy LWL Algorithm

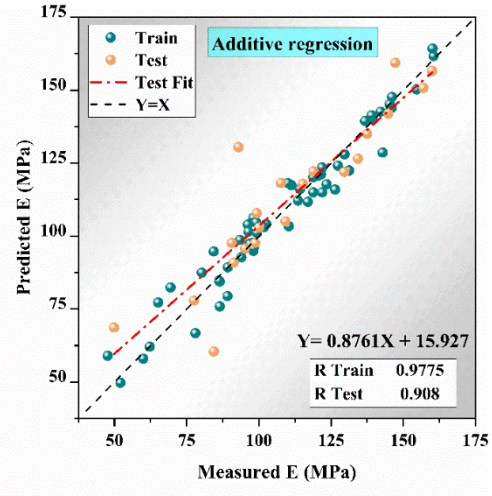

(a)

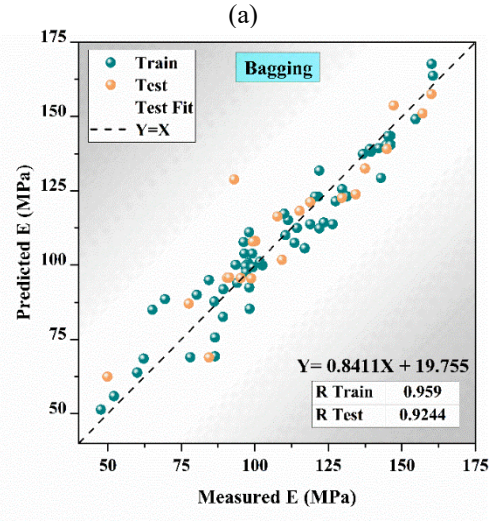

(b)

Fig. 15 The squared correlation coefficient for Hybrid Meta classifiers models: (a) AR-GPR, and (b) BAG-GPR

3.2 Sensitivity analysis

An assessment of the single and hybrid forecasting models' sensitivity was carried out to evaluate the most efficient input parameters to compute the E of frozen sand. Various training data were built by removing a single input parameter simultaneously, and the test data set reported the amounts of four statistical performance criteria as R2, RMSE, MAE, and MAPE. According to the previous sections, the data set is divided into 75% and 25% for training and testing, respectively. The best model for the sensitivity analysis is chosen using the statistical performance criteria. In this study, the MLP single model is considered because of the good performance. The results are presented in Table 7, which is shown that the Temperature (T) is the most effective parameter to forecast the E of frozen sand using the mentioned model. From this aspect, Cell Pressure (CP), time (t), Strain (S), and Strain Rate (SR) are in the following ranks, respectively however they are not as effective as T.

It is worth mentioning that eliminating input variables may only cause a minimal performance loss for the model, but in the present study, because the analysis was based upon the results of experimental measurements so as to specify the impressions of replacement materials on the E of frozen sand, eliminating variable may reject the generalizability of the model. Taking into account the multicollinearity problem has not a significant impact on the fit of a model and also commonly does not impress remarkably on predictions (Kutner *et al.* 2004), the present study does not prefer deleting any variable.

4. Conclusions

This study presents a comprehensive data-mining-based model for predicting the Young's Modulus of frozen sand under the triaxial test. For the prediction purposes, different models were considered including additive regression, bagging, M5-Rules, M5P, random forests, support vector regression, locally weighted linear, gaussian process regression, and multi-layered perceptron neural network. Based on the results of the experimental study in determining the E of the frozen sand and the results of the predictions via nine single and hybrid models conducted in the present study following conclusions are drawn:

- Based on the prediction of training data, the MLP and GPR techniques have the best and the worst performance in predicting the E of frozen sand among all nine models, respectively.
- Considering the R2 and RMSE in function models, MLP, SVR, and GPR have the best, acceptable, and the worst accuracy in forecasting the training data, respectively. Reflecting the MAE in function models, MLP, SVR, and GPR have the best, very well, and the worst outputs in forecasting the training data. With regard to MAPE in function models MLP, SVR, and GPR have excellent, very well and weak outputs in predicting the training data.
- Based on training data the best performances of R2, RMSE, MAE and MAPE are relevant to MLP, MLP, MLP and AR-GPR, respectively. Based upon testing data the best performances of R2, RMSE, MAE and MAPE are related to BAG-GPR, BAG-GPR, AR-GPR and AR-GPR, respectively.

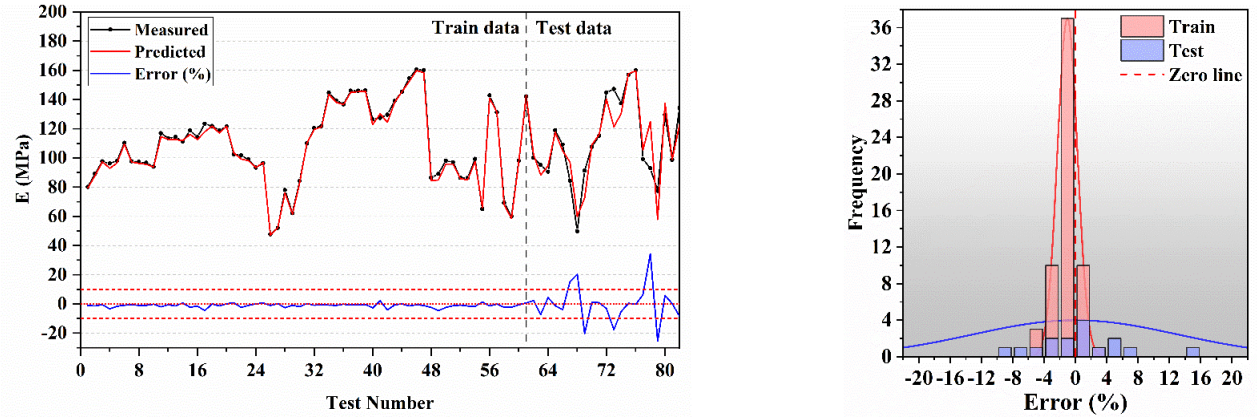

Fig. 16 Predicted E of frozen sand, Error and Normal distribution for MLP model

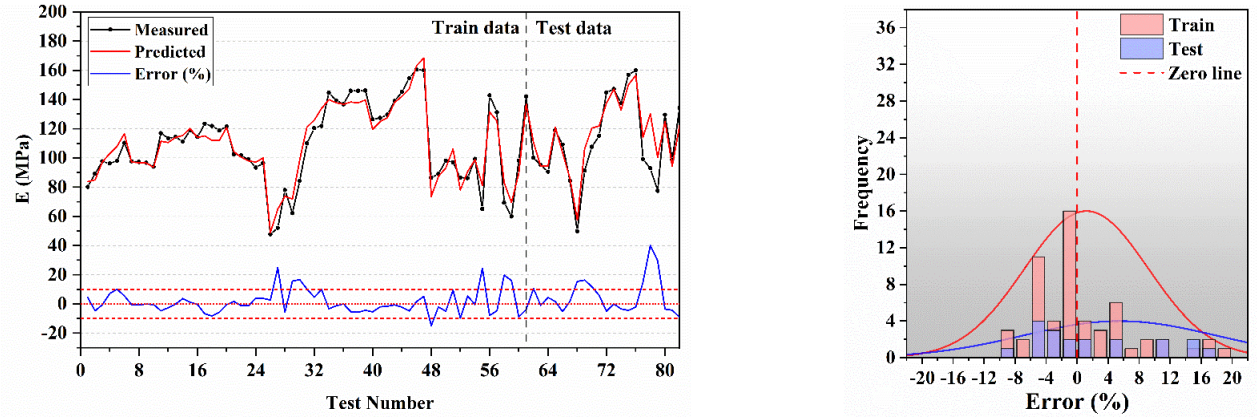

Fig. 17 Predicted E of frozen sand, Error and Normal distribution for M5P model

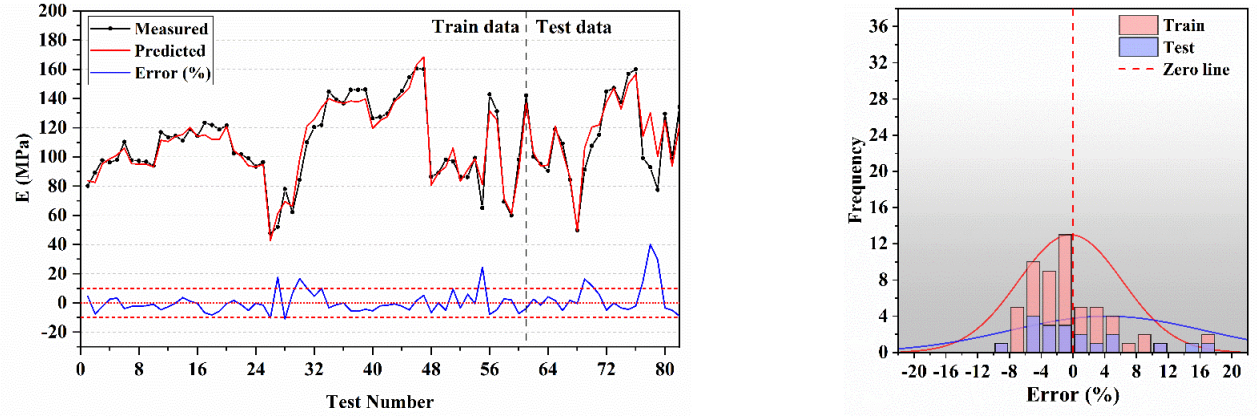

Fig. 18 Predicted E of frozen sand, Error and Normal distribution for M5R model

Table 7 Sensitivity analysis using the tree-based RF model

No.	Inputs	Removed parameter	R^2	RMSE	MAE	MAPE	Total Ranking
1	T, CP, SR, S, t	-	0.9973	1.7533	1.3322	0.000098	-
2		T	0.1904	28.0689	24.8303	0.0162	1
3		CP	0.7443	14.098	10.9124	0.008	2
4		SR	0.8782	10.0031	6.5593	0.0013	5
5		S	0.8207	11.7583	9.365	0.0066	4
6		t	0.798	12.9465	8.3502	0.0033	3

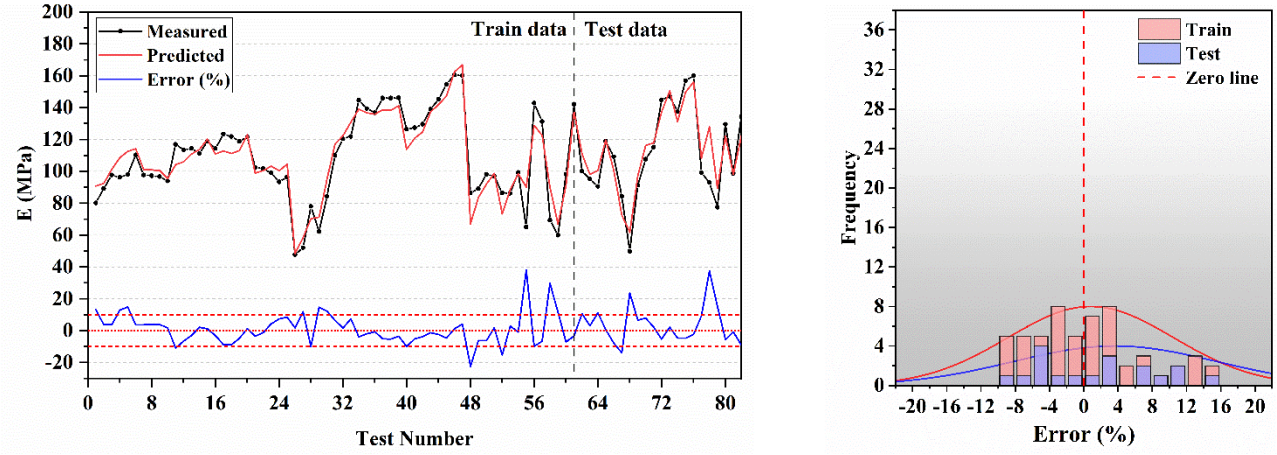

Fig. 19 Predicted E of frozen sand, Error and Normal distribution for GPR model

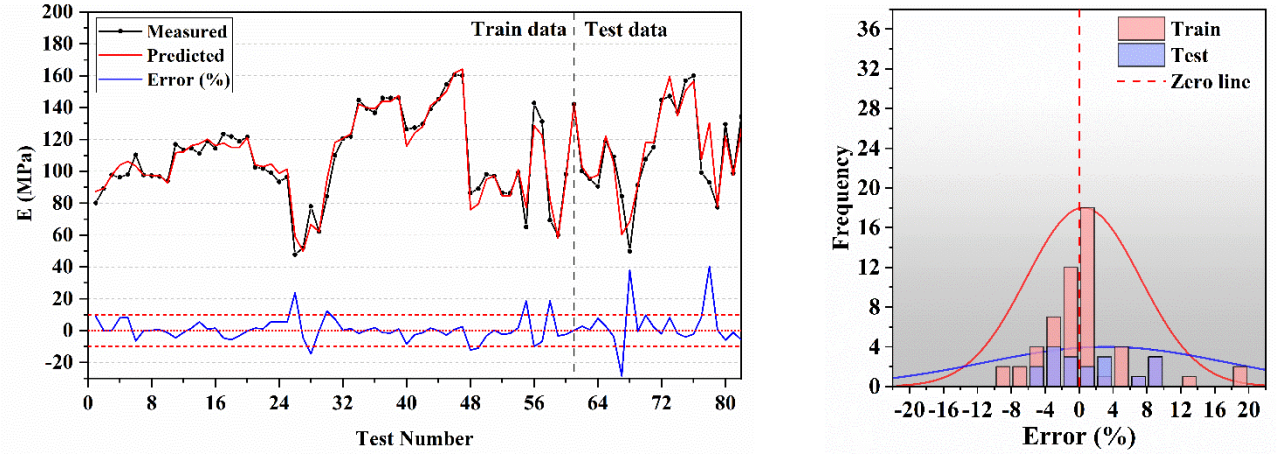

Fig. 20 Predicted E of frozen sand, Error and Normal distribution for Hybrid AR-GPR model

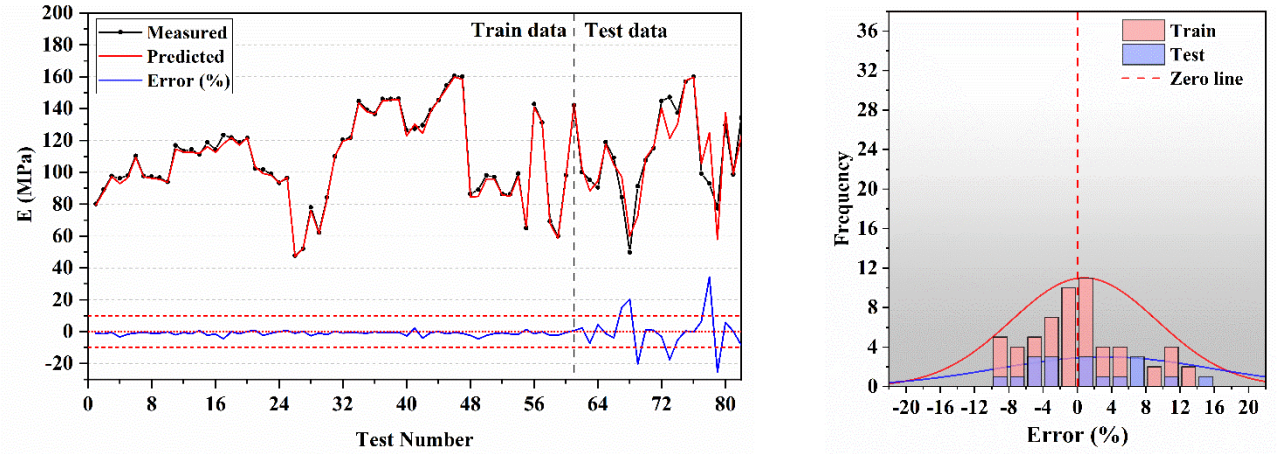

Fig. 21 Predicted E of frozen sand, Error and Normal distribution for LWL model

References

Akhtar, S. and Li, B. (2020), "Numerical analysis of pipeline uplift resistance in frozen clay soil considering hybrid tensile-shear yield behaviors", *Int. J. Geosynthetics Ground Eng.*, **6**(4), 1-12. https://doi.org/10.1007/s40891-020-00228-9.

Alzabeebee, S., Zuhaira, A.A. andAl-Hamd, R.K.S. (2022), "Development of an optimized model to compute the undrained shaft friction adhesion factor of bored piles", *Geomech. Eng.*, **28**(4), 397-404. https://doi.org/10.12989/gae.2022.28.4.397.

Andersland, O.B. and Ladanyi, B. (2013), "An introduction to frozen ground engineering", *Springer Science & Business Media*, https://doi.org/10.1007/978-1-4757-2290-1-3.

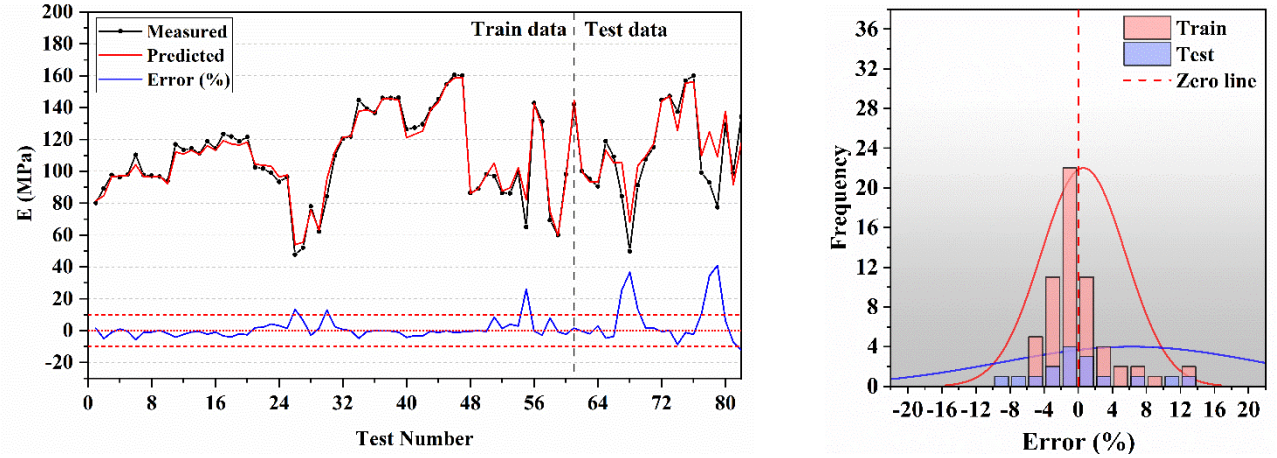

Fig. 22 Predicted E of frozen sand, Error and Normal distribution for RF model

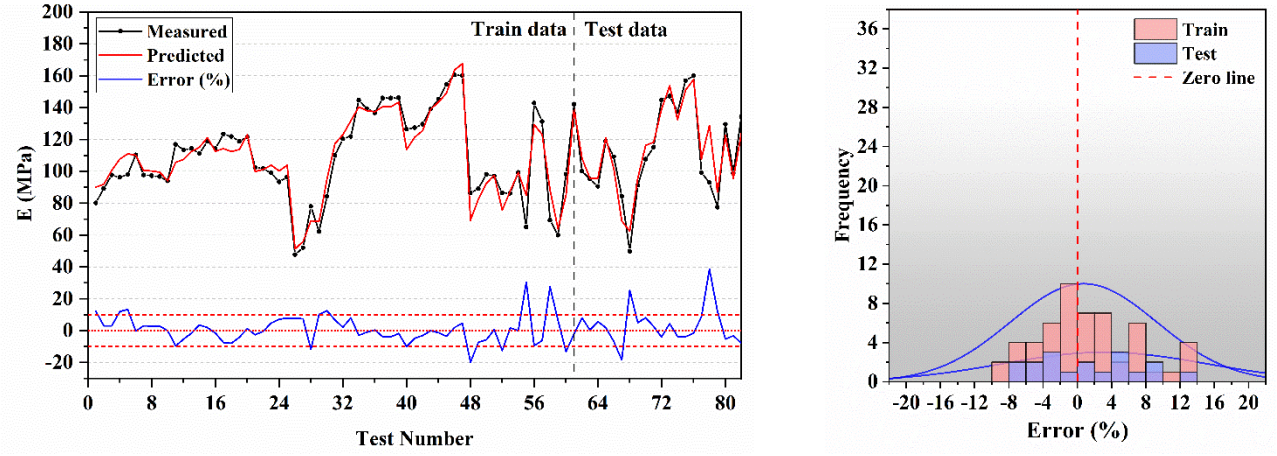

Fig. 23 Predicted E of frozen sand, Error and Normal distribution for Hybrid BAG-GPR model

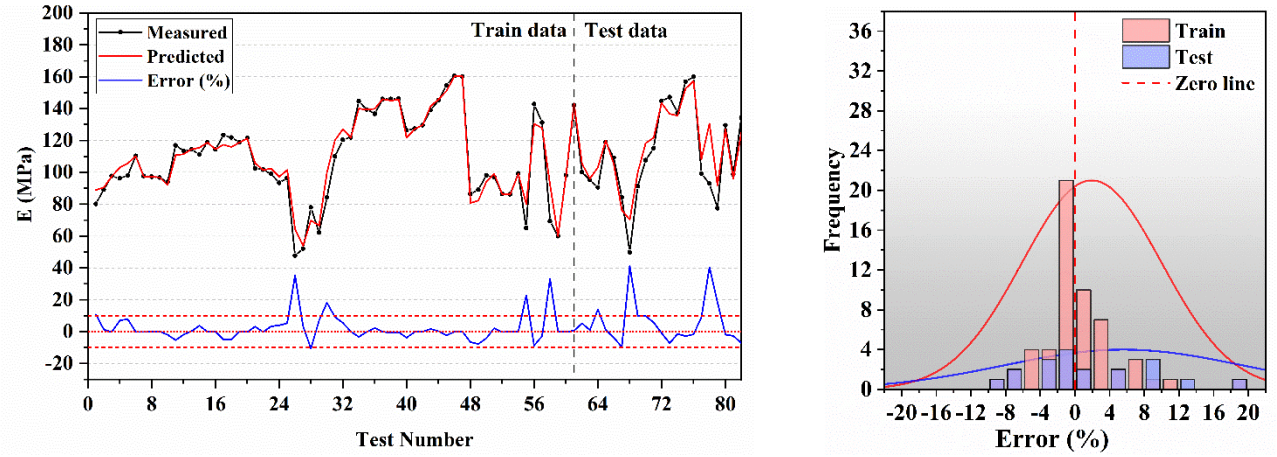

Fig. 24 Predicted E of frozen sand, Error and Normal distribution for SVR model

Atkeson, C.G., Moore, A.W. and Schaal, S. (1997), "Locally weighted learning", *Lazy learning*, 11-73. https://doi.org/10.1007/978-94-017-2053-3.

Bakermans, L. and Jamieson, B. (2009), "SWarm: A simple regression model to estimate near-surface snowpack warming for back-country avalanche forecasting", *Cold Reg. Sci. Technol.*, **59**(2-3), 133-142. https://doi.org/10.1016/j.coldregions.2009.06.003

Bayram, F. (2012), "Predicting mechanical strength loss of natural stones after freeze–thaw in cold regions", *Cold Reg. Sci. Technol.*, **83**, 98-102. https://doi.org/10.1016/j.coldregions.2012.07.003.

Bean, B., Maguire, M. and Sun, Y. (2019), "Comparing design ground snow load prediction in Utah and Idaho", *J. Cold Reg.*

Eng., **33**(3), 04019010. https://doi.org/10.1061/(ASCE)CR.1943-5495.000019.

Bishop, C.M. (1995), "Neural networks for pattern recognition", *Oxford University Press*. https://dl.acm.org/doi/10.5555/525960.

Breiman, L. (1996), "Bagging predictors", *Machine learning*, **24**(2), 123-140. https://doi.org/10.1007/BF0005865.

Breiman, L. (2001), "Random forests", *Machine learning*, **45**(1), 5-32. https://doi.org/10.1023/A:1010933404324.

Chai, M., Zhang, H., Zhang, J. and Zhang, Z. (2017), "Effect of cement additives on unconfined compressive strength of warm and ice-rich frozen soil", *Constr. Build. Mater.*, **149**, 861-868. https://doi.org/10.1016/j.conbuildmat.2017.05.202.

Chen, T., Morris, J. and Martin, E. (2007), "Gaussian process regression for multivariate spectroscopic calibration", *Chemometrics and Intelligent Laboratory Systems*, **87**(1), 59-71. https://doi.org/10.1016/j.chemolab.2006.09.004

Dehghanbanadaki, A., Rashid, A.S.A., Ahmad, K., Yunus, N.Z. M. and Said, K.N.M. (2022), "A computational estimation model for the subgrade reaction modulus of soil improved with DCM columns", *Geomech. Eng.*, **28**(4), 385-396. https://doi.org/10.12989/gae.2022.28.4.385.

Deka, P.C. (2014), "Support vector machine applications in the field of hydrology: a review", *Appl. Soft Comput.*, **19**, 372-386. https://doi.org/10.1016/j.asoc.2014.02.002.

Dawei, Y., Bing, Z., Bingbing, G., Xibo, G. and Razzaghzadeh, B. (2023), "Predicting the CPT-based pile set-up parameters using HHO-RF and PSO-RF hybrid models", *Struct. Eng. Mech.*, **86**(5), 673-686. https://doi.org/10.12989/sem.2023.86.5.673.

Dinarvand, R. and Ardakani, A. (2022), "Shear behavior of geotextile-encased gravel columns in silty sand-Experimental and SVM modeling", *Geomech. Eng.*, **28**(5), 505-520. https://doi.org/10.12989/gae.2022.28.5.505.

Esmaeili-Choobar, N., Esmaeili-Falak, M., Roohi-hir, M. and Keshtzad, S. (2013), "Evaluation of collapsibility potential at Talesh, Iran", *Electronic J. Geotech. Eng*., **18**, 2561-2573.

Esmaeili-Falak, M. and Hajialilue-Bonab, M. (2012), "Numerical studying the effects of gradient degree on slope stability analysis using limit equilibrium and finite element methods", *Int. J. Academic Res.*, **4**(6), 216-222.

Esmaeili-Falak, M., Katebi, H. and Javadi, A. (2018), "Experimental study of the mechanical behavior of frozen soils-A case study of Tabriz subway", *Periodica Polytechnica Civil Eng.*, **62**(1), 117-125. https://doi.org/10.3311/PPci.10960.

Esmaeili-Falak, M., Katebi, H., Vadiati, M. and Adamowski, J. (2019), "Predicting triaxial compressive strength and Young's modulus of frozen sand using artificial intelligence methods", *J. Cold Reg. Eng.*, **33**(3), 04019007. https://doi.org/10.1061/(ASCE)CR.1943-5495.0000188.

Esmaeili-Falak, M. and Sarkhani Benemaran, R. (2023), "Ensemble deep learning-based models to predict the resilient modulus of modified base materials subjected to wet-dry cycles", *Geomech. Eng.*, **32**(6), 583-600. https://doi.org/10.12989/gae.2023.32.6.583.

Esmaeili-Falak, M. and Sarkhani Benemaran, R. (2022), "Investigating the stress-strain behavior of frozen clay using triaxial test", *J. Struct. Constr. Eng*., https://doi.org/10.22065/JSCE.2022.332406.2747.

Fei, W. and Yang, Z.J. (2019), "Modeling unconfined compression behavior of frozen Fairbanks silt considering effects of temperature, strain rate and dry density", *Cold Reg. Sci. Technol.*, **158**, 252-263. https://doi.org/10.1016/j.coldregions.2018.09.002.

Frank, E. and Witten, I.H. (1998), "Generating accurate rule sets without global optimization", https://dl.acm.org/doi/10.5555/645527.657305

Friedman, J.H. (2001), "Greedy function approximation: a gradient boosting machine", *Annals Statistics*, 1189-1232. https://doi.org/10.1214/aos/1013203451.

Friedman, J.H. and Meulman, J.J. (2003), "Multiple additive regression trees with application in epidemiology", *Stat. Med.*, **22**(9), 1365-1381. https://doi.org/10.1002/sim.1501.

Fu, H., Zhang, J., Huang, Z., Shi, Y. and Chen, W. (2018), "A statistical model for predicting the triaxial compressive strength of transversely isotropic rocks subjected to freeze–thaw cycling", *Cold Reg. Sci. Technol.*, **145**, 237-248. https://doi.org/10.1016/j.coldregions.2017.11.003.

Ge, D.M., Zhao, L.C. and Esmaeili-Falak, M. (2022), "Estimation of rapid chloride permeability of SCC using hyperparameters optimized random forest models", *J. Sustain. Cement-Based Mater.*, 1-19. https://doi.org/10.1080/21650373.2022.2093291.

Goughnour, R.R. and Andersland, O.B. (1968), "Mechanical properties of a sand-ice system", *J Soil Mech. Found. Division*, **94**(4), 923-950. https://doi.org/10.1061/JSFEAQ.0001179.

Habibagahi, G., Katebi, S. and Johari, A. (2020), "A neural network framework for unsaturated soils", *Unsaturated Soils for Asia*, 107-111.

Holmes, G., Hall, M. and Prank, E. (1999), "Generating rule sets from model trees", *Proceedings of the Australasian joint conference on artificial intelligence*, Berlin, Heidelberg. https://doi.org/10.1007/3-540-46695-9-1

Hou, C., Zhu, W., Yan, B., Guan, K. and Du, J. (2020), "The effects of temperature and binder content on the behavior of frozen cemented tailings backfill at early ages", *Constr. Build. Mater.*, **239**, 117752. https://doi.org/10.1016/j.conbuildmat.2019.117752.

Huang, S., Guo, Y., Liu, Y., Ke, L. and Liu, G. (2018), "Study on the influence of water flow on temperature around freeze pipes and its distribution optimization during artificial ground freezing", *Appl. Therm. Eng.*, **135**, 435-445. https://doi.org/10.1016/j.applthermaleng.2018.02.090.

Jamshidi, A., Nikudel, M.R. and Khamehchiyan, M. (2013), "Predicting the long-term durability of building stones against freeze–thaw using a decay function model," *Cold Reg. Sci. Technol.*, **92**, 29-36. https://doi.org/10.1016/j.coldregions.2013.03.007.

Johari, A. and Fooladi, H. (2020), "Comparative study of stochastic slope stability analysis based on conditional and unconditional random field", *Comput. Geotech.*, **125**, 103707. https://doi.org/10.1016/j.compgeo.2020.103707.

Johari, A. and Fooladi, H. (2022), "Simulation of the conditional models of borehole's characteristics for slope reliability assessment", *Transport. Geotech.*, 100778. https://doi.org/10.1016/j.trgeo.2022.100778.

Johari, A. and Golkarfard, H. (2018), "Reliability analysis of unsaturated soil sites based on fundamental period throughout Shiraz, Iran", *Soil Dyn. Earthq. Eng.*, **115**, 183-197. https://doi.org/10.1016/j.soildyn.2018.08.012.

Johari, A., Golkarfard, H., Davoudi, F. and Fazeli, A. (2021a), "A predictive model based on the experimental investigation of collapsible soil treatment using nano-clay in the Sivand Dam region, Iran", *Bull. Eng. Geol. Environ.*, **80**(9), 6725-6748. https://doi.org/10.1007/s10064-021-02360-w.

Johari, A., Habibagahi, G. and Ghahramani, A. (2006), "Prediction of soil–water characteristic curve using genetic programming", *J. Geotech. Geoenviron. Eng.*, **132**(5), 661-665. https://doi.org/10.1061/(ASCE)1090-0241(2006)132:5(661).

Johari, A., Habibagahi, G. and Ghahramani, A. (2011), "Prediction of SWCC using artificial intelligent systems: A comparative study", *Scientia Iranica*, **18**(5), 1002-1008. https://doi.org/10.1016/j.scient.2011.09.002.

Johari, A., Heydari, A. and Talebi, A. (2021b), "Prediction of discharge flow rate beneath sheet piles using scaled boundary finite element modeling database", *Scientia Iranica*, **28**(2), 645-655. https://doi.org/10.24200/SCI.2020.53281.3158.

Kim, Y., Hong, J., Shin, J. and Kim, B. (2022), "Shield TBM disc cutter replacement and wear rate prediction using machine learning techniques", *Geomech. Eng.*, **29**(3), 249-258. https://doi.org/10.12989/gae.2022.29.3.249.

Kotilainen, M., Vanhatalo, J., Suominen, M. and Kujala, P. (2017), "Predicting ice-induced load amplitudes on ship bow conditional on ice thickness and ship speed in the Baltic Sea", *Cold Reg. Sci. Technol.*, **135**, 116-126. https://doi.org/10.1016/j.coldregions.2016.12.006.

Kwak, N.S. and Ko, T.Y. (2022), "Machine learning-based regression analysis for estimating Cerchar abrasivity index", *Geomech. Eng.*, **29**(3), 219-228. https://doi.org/10.12989/gae.2022.29.3.219.

Lawal, A.I., Kwon, S., Aladejare, A.E. and Oniyide, G.O. (2022), "Prediction of the static and dynamic mechanical properties of sedimentary rock using soft computing methods", *Geomech. Eng.*, **28**(3), 313-324. https://doi.org/10.12989/gae.2022.28.3.313.

Mahmoodzadeh, A., Mohammadi, M., Abdulhamid, S.N., Ali, H. F.H., Ibrahim, H.H. and Rashidi, S. (2022a), "Forecasting tunnel path geology using Gaussian process regression", *Geomech. Eng.*, **28**(4), 359-374. https://doi.org/10.12989/gae.2022.28.4.359.

Mahmoodzadeh, A., Mohammadi, M., Abdulhamid, S.N., Ibrahim, H.H., Ali, H.F.H., Nejati, H.R. and Rashidi, S. (2022b), "Prediction of duration and construction cost of road tunnels using Gaussian process regression", *Geomech. Eng.*, **28**(1), 65-75. https://doi.org/10.12989/gae.2021.28.1.065.

Misra, S. and Li, H. (2019), "Noninvasive fracture characterization based on the classification of sonic wave travel times", *Machine Learning for Subsurface Characterization*, 243-287. https://doi.org/10.1016/C2018-0-01926-X.

Mohan L,G., Rasheed, D.K. and Zachariah Koshy, D. (2019), "Experimental investigation on shear strength of artificially frozen C–Phi soil", *Int. J. Adv. Res. Eng. Technol.*, **10**(3). https://doi.org/10.34218/IJARET.10.3.2019.005.

Moradi, G., Hassankhani, E. and Halabian, A.M. (2022), "Experimental and numerical analyses of buried box culverts in trenches using geofoam", *Proceedings of the Institution of Civil Engineers-Geotechnical Engineering*, **175**(3), 311-322.

Morgan, J.N. and Sonquist, J.A. (1963), "Problems in the analysis of survey data, and a proposal", *J. Am. Stat. Association*, **58**(302), 415-434. https://doi.org/10.2307/2283276.

Nassr, A., Esmaeili-Falak, M., Katebi, H. and Javadi, A. (2018), "A new approach to modeling the behavior of frozen soils," *Eng. Geol.*, **246**, 82-90. https://doi.org/10.1016/j.enggeo.2018.09.018.

Omran, B.A., Chen, Q. and Jin, R. (2016), "Comparison of data mining techniques for predicting compressive strength of environmentally friendly concrete", *J. Comput Civil Eng.*, **30**(6), 04016029. https://doi.org/10.1061/(ASCE)CP.1943-5487.0000596.

Platt, J. (1998), "Sequential minimal optimization: A fast algorithm for training support vector machines".

Quinlan, J.R. (1992), "Learning with continuous classes", *Proceedings of the 5th Australian joint conference on artificial intelligence*, **92**, 343-348. https://doi.org/10.1142/9789814536271.

Rao, S.B. (1986), "Tool wear monitoring through the dynamics of stable turning". https://doi.org/10.1115/1.3187062

Sarkhani Benemaran, R., Esmaeili-Falak, M. and Javadi, A. (2022), "Predicting resilient modulus of flexible pavement foundation using extreme gradient boosting based optimized models", *Int. J. Pavement Eng.*, 1-19. https://doi.org/10.1080/10298436.2022.2095385.

Sarkhani Benemaran, R., Esmaeili-Falak, M. andKatebi, H. (2022), "Physical and numerical modelling of pile-stabilised saturated layered slopes", *Proceedings of the Institution of Civil Engineers-Geotechnical Engineering*, **175**(5), 523-538. https://doi.org/10.1680/jgeen.20.00152.

Soquist, J.N. and Morgabn, J.N. (1964), "The detection of interaction effects", **35**. *Survey Research Center, Institute for Social Research*, University of Michigan.

Sun, Q. and Liu, C. (2022), "Near-explosion protection method of π-section reinforced concrete beam", *Geomech. Eng.*, **28**(3), 209-224. https://doi.org/10.12989/gae.2022.28.3.209.

Török, Á., Ficsor, A., Davarpanah, M. and Vásárhelyi, B. (2019), "Comparison of mechanical properties of dry, Saturated and frozen porous rocks", *Proceedings of the IAEG/AEG Annual Meeting Proceedings*, San Francisco, California, *Springer, Cham*, **6**, 113-118. https://doi.org/10.1007/978-3-319-93142-5-16

Vahdani, M., Ghazavi, M. and Roustaei, M. (2020), "Prediction of mechanical properties of frozen soils using response surface method: An optimization Approach", *Int. J. Eng.*, **33**(10), 1826-1841. https://doi.org/10.5829/IJE.2020.33.10A.02.

Van Eck, N.A. (1980), "Statistical analysis and data management highlights of OSIRIS IV", *The American Statistician*, **34**(2), 119-121. https://doi.org/10.1016/0167-9473(83)90066-X .

Vanthienen, J. and Wets, G. (1994), "From decision tables to expert system shells", *Data & Knowledge Eng.*, **13**(3), 265-282. https://doi.org/10.1016/0169-023X(94)00020-4.

Vapnik, V. (2013), "The nature of statistical learning theory", *Springer Science & Business Media.* https://doi.org/10.1007/978-1-4757-3264-1

Wang, B. and Chen, T. (2015), "Gaussian process regression with multiple response variables", *Chemometrics and Intelligent Laboratory Systems*, **142**, 159-165. https://doi.org/10.1016/j.chemolab.2015.01.016.

Wang, T., Ma, H., Liu, J., Luo, Q., Wang, Q. and Zhan, Y. (2021), "Assessing frost heave susceptibility of gravelly soils based on multivariate adaptive regression splines model", *Cold Reg. Sci. Technol.*, **181**, 103182. https://doi.org/10.1016/j.coldregions.2020.103182.

Witten, I.H., Frank, E., Hall, M.A. and Pal, C.J. (2005), "Practical machine learning tools and techniques", *Morgan Kaufmann*, **578**. https://doi.org/10.1016/C2009-0-19715-5 .

Wood, D.M. (2003), "Geotechnical modelling (Vol. 1). *CRC press*. https://doi.org/10.1201/9781315273556.

Yan, Y. (2022), "Resonance frequency and stability of composite micro/nanoshell via deep neural network trained by adaptive momentum-based approach", *Geomech. Eng.*, **28**(5), 477-491. https://doi.org/10.12989/gae.2022.28.5.477.

Yang, X., You, Z., Hiller, J. and Watkins, D. (2017), "Correlation analysis between temperature indices and flexible pavement distress predictions using mechanistic-empirical design", *J. Cold Reg. Eng.*, **31**(4), 04017009. https://doi.org/10.1061/(ASCE)CR.1943-5495.0000135.

Zhang, D.M., Xie, X.C., Li, Z.L. and Zhang, J. (2020), "Simplified analysis method for predicting the influence of deep excavation on existing tunnels", *Comput. Geotech.*, **121**, 103477. https://doi.org/10.1016/j.compgeo.2020.103477.

Zhang, G., Chen, C., Zhang, Y., Zhao, H., Wang, Y. and Wang, X. (2022), "Optimised neural network prediction of interface bond strength for GFRP tendon reinforced cemented soil", *Geomech. Eng.*, **28**(6), 599-611. https://doi.org/10.12989/gae.2022.28.6.599.

Zhu, Y., Huang, L., Zhang, Z. and Bayrami, B. (2022), "Estimation of splitting tensile strength of modified recycled aggregate concrete using hybrid algorithms", *Steel Compos. Struct.*, **44**(3), 375-392. https://doi.org/10.12989/scs.2022.44.3.389.

GC

Nomenclature

AGF	Artificial Ground Freezing
AR	Additive Regression
BAG	Bagging
M5R	M5-Rules
RF	Random Forest
SVR	Support Vector Regression
LWL	Locally Weighted Linear
GPR	Gaussian Process Regression
MLP	Multilayer Perceptron
SVM	Support Vector Machine
$RMSE$	Root Mean Squared Error
MAE	Mean Absolute Error
PI	Performance Index
VAF	Variance Account Factor
RMSE	Root Mean Squared Error
R^2	Squared Coefficient of Determination
MAE	Mean Absolute Error
MAPE	Mean Absolute Percentage Error
T	Temperature
SR	Strain Rate
CP	Cell Pressure
E	Young's Modulus
t	Time
S	Strain